CELLULAR NEUROSCIENCE

Dynamin controls neuropeptide secretion by organizing dense-core vesicle fusion sites

Alessandro Moro[1,2], Anne van Nifterick[2], Ruud F. Toonen[2]*, Matthijs Verhage[1,2]*

Synaptic vesicles (SVs) release neurotransmitters at specialized active zones, but release sites and organizing principles for the other major secretory pathway, neuropeptide/neuromodulator release from dense-core vesicles (DCVs), remain elusive. We identify dynamins, yeast Vps1 orthologs, as DCV fusion site organizers in mammalian neurons. Genetic or pharmacological inactivation of all three dynamins strongly impaired DCV exocytosis, while SV exocytosis remained unaffected. Wild-type dynamin restored normal exocytosis but not guanosine triphosphatase–deficient or membrane-binding mutants that cause neurodevelopmental syndromes. During prolonged stimulation, repeated use of the same DCV fusion location was impaired in dynamin 1-3 triple knockout neurons. The syntaxin-1 staining efficiency, but not its expression level, was reduced. αSNAP (α–soluble *N*-ethylmaleimide–sensitive factor attachment protein) expression restored this. We conclude that mammalian dynamins organize DCV fusion sites, downstream of αSNAP, by regulating the equilibrium between fusogenic and non-fusogenic syntaxin-1 promoting its availability for SNARE (SNAP receptor) complex formation and DCV exocytosis.

INTRODUCTION

Neurons send chemical signals to their environment primarily using two specialized secretory pathways: synaptic vesicle (SV) exocytosis, which accounts for fast synaptic transmission (*1*, *2*), and neuropeptide/neuromodulator secretion from dense-core vesicles (DCVs). In contrast to SVs, DCVs do not recycle locally but are continuously generated de novo at the Golgi apparatus (*3*–*5*). Whereas SVs release neurotransmitters at specialized presynaptic sites, the active zones, DCVs release neuromodulators throughout the neuron, both at synapses and outside synapses (*6*–*9*). The determinants of DCV fusion sites are unknown.

In mouse hippocampal neurons, DCV exocytosis is predominantly axonal (*8*), although release from dendrites may be more efficient due to longer fusion pore opening (*10*). In contrast, hypothalamic and raphe nucleus neurons show strong preference for dendritic DCV exocytosis (*11*). Neuromodulators such as oxytocin and dopamine are proposed to depend on volume transmission (*12*) and use transient fusion sites (*13*, *14*). Although fusion sites are poorly defined, DCV fusion is known to use largely the same release machinery as SVs, such as the neuronal SNARE [soluble *N*-ethylmaleimide–sensitive factor (NSF) attachment protein (SNAP) receptor] proteins SNAP-25 and synaptobrevin/VAMP2, and key SNARE regulators such as Munc13 and RIM (*6*, *15*–*18*). How these components are brought together (transiently) to form DCV fusion sites remains elusive.

The aim of this study was to elucidate such principles and to identify components that organize DCV fusion sites. As a starting point, we used conserved principles elucidated in yeast *Saccharomyces cerevisiae*, where the guanosine triphosphatase (GTPase) Vps1 promotes vacuolar fusion by binding the SNARE protein Vam3p (a syntaxin ortholog) (*19*) and recruiting a tethering complex (*20*–*22*). Mammals express three Vps1 orthologs, dynamins 1 to 3, known to catalyze fission of budding endocytic vesicles (*23*–*25*). In neurons, dynamin 1 is the main isoform and, together with dynamin 3, regulates SV endocytosis (*25*–*28*), while dynamin 2 is responsible for generic, clathrin-mediated endocytosis and the early stage of brain development (*29*). However, in chromaffin cells, dynamin is also present at the plasma membrane before fusion of secretory vesicles (*30*), and dynamin 2 influences insulin release in pancreatic cells (*31*, *32*). Furthermore, endophilin, which facilitates dynamin association to the plasma membrane (*29*, *33*–*35*), was recently reported to promote neurosecretory vesicle exocytosis in chromaffin cells (*36*), suggesting that mammalian dynamins may also have retained a Vps1-like role in the organization of transient fusion sites. In this study, dynamin 1, 2, and 3 triple knockout (TKO) neurons were used to investigate the role of dynamins in DCV fusion in mouse hippocampal neurons. We show that, independently of their role in SV endocytosis, dynamins are major regulators of DCV exocytosis. Genetic perturbation and acute pharmacological inhibition of dynamin both resulted in strongly impaired DCV fusion, especially during prolonged stimulation. Whereas DCVs often fuse at the same locations in wild-type (WT) neurons during prolonged stimulation, repeated use of the same locations was reduced in the absence of dynamins. In TKO neurons, the accessibility of the mammalian Vam3p ortholog syntaxin-1, but not its absolute expression level, was considerably reduced. This reduced accessibility was restored by αSNAP overexpression. We conclude that dynamin is an important regulator of DCV fusion by promoting the assembly of the t-SNARE syntaxin-1 into fusion sites, allowing the formation of *trans*-SNAREs and DCV exocytosis.

RESULTS

Dynamin is required for normal neurite extension but dispensable for SV exocytosis

To test whether dynamins regulate DCV release sites in mammalian neurons, we used *Dnm1*$^{+/-}$; *Dnm2*$^{lox/lox}$; *Dnm3*$^{-/-}$ mice (*37*) to generate dynamin 3 KO and dynamin 1 and 3 DKO (double KO) neuronal

[1]Department of Clinical Genetics, Center for Neurogenomics and Cognitive Research (CNCR), Amsterdam Neuroscience, VU University Medical Center, Amsterdam, Netherlands. [2]Department of Functional Genomics, Center for Neurogenomics and Cognitive Research (CNCR), Vrije Universiteit (VU) Amsterdam, de Boelelaan 1087, 1081 HV Amsterdam, Netherlands.
*Corresponding author. Email: matthijs@cncr.vu.nl (M.V.); ruud.toonen@cncr.vu.nl (R.F.T.)

cultures. The latter were infected at 9 days in vitro (DIV 9) with Cre recombinase to obtain dynamin 1 to 3 TKO neurons at DIV 15 (Fig. 1A).

To first assess potential generic effects of dynamin gene inactivation on neuronal morphology and DCV biogenesis, DIV 15 neurons were immunostained for the dendritic marker MAP2, the SV marker synaptophysin (Syp1), and the DCV marker chromogranin-B (CHGB) (Fig. 1B) (*8*). Despite shorter dendrite length (Fig. 1C), synapse density was unchanged in TKO cultures compared to DKO and 20% reduced compared to dynamin 3 single KO (Fig. 1D). Chromogranin-B puncta density, as well as intensity of synaptophysin and Chromogranin-B in synapses, was comparable between all three genotypes (Fig. 1, E to G). Ca^{2+} responses to repetitive stimulation, as a measure of neuronal viability, showed similar kinetics in all genotypes (fig. S1, C and D), including a rapid decay after peak Ca^{2+} increases (fig. S1E). Significant neuronal degeneration started only at 6 days after infection with Cre recombinase (fig. S1B). These data suggest that a minimal level of dynamin expression is required for neuronal survival but that neurons are healthy up to 6 days after Cre infection and contain a normal number of DCVs.

Next, we examined SV exocytosis and endocytosis upon 5 s of 40-Hz electrical stimulation in dynamin TKO neurons, using Synaptophysin-pHluorin (SypHy; Fig. 1H) (*38*). SV release probability, expressed as a ratio between the maximum fluorescence signal upon stimulation and the fluorescence upon brief superfusion of Tyrode's solution containing NH_4Cl, was comparable between the three genotypes (Fig. 1J). As expected, SV endocytosis was blocked both in DKO and TKO synapses (Fig. 1, K and I). Together, these data show that inactivation of all dynamin genes does not affect SV exocytosis, DCV numbers, and calcium handling up to 6 days after Cre expression, while, as expected, SV endocytosis is blocked in dynamin DKO and TKO neurons.

Dynamin is a major regulator of DCV exocytosis

To test whether inactivation of dynamin genes affects DCV exocytosis, neurons were infected with the DCV fusion reporter NPY-super-ecliptic-pHluorin (SEP) (*7*). The total number of NPY-SEP vesicles was similar between the three genotypes (Fig. 2E), in line with the normal puncta density of endogenous chromogranin-B (Fig. 1G). Evoked DCV exocytosis was quantified during two bursts of eight trains of 50 action potentials (APs) at 50 Hz (Fig. 2, A to C) (*8*, *39*). Dynamin 3 KO cultures were used as littermate controls since DCV exocytosis in these neurons was similar to that in WT neurons (Fig. 3D).

DCV exocytosis in dynamin TKO neurons was strongly impaired as compared to dynamin 1 and 3 DKO and dynamin 3 KO neurons (Fig. 2, B to D). During the first four AP trains, DCV exocytosis in TKO neurons was similar to the control dynamin 3 KO neurons (Fig. 2G). However, during prolonged stimulation DCV fusion was markedly impaired, resulting in a ~60% overall reduction (Fig. 2H). DCV exocytosis was not reduced in dynamin 1 and 3 DKO neurons, despite the block of SV endocytosis (Fig. 1, I to K). DCV exocytosis was even increased in DKO neurons during the first two trains (Fig. 2G). Consequently, the average delay between the start of the stimulation and the DCV fusion events was significantly decreased (fig. S3, F and G).

To confirm the strong impairment of DCV exocytosis observed with NPY-SEP, brain-derived neurotrophic factor (BDNF)–SEP was used as an independent reporter in a separate set of experiments. Using this reporter, a similar impairment in DCV exocytosis was observed in dynamin TKO neurons but, again, not in DKO neurons (fig. S3, A to E).

To test whether the exocytosis defects were specifically related to dynamin 1 and/or 2, we quantified DCV exocytosis in each individual dynamin KO (Fig. 3). Whereas dynamin 1 single KO had a similar effect in increasing DCV exocytosis during the first phase of the stimulation, as observed in dynamin 1 and 3 DKO neurons, only dynamin TKO neurons showed a marked decrease in DCV exocytosis that was not replicated by any individual KO (Fig. 3, A and B). In addition, both dynamins 1 and 2 alone rescued the DCV fusion deficit of TKO neurons (Fig. 3, E and F). These data indicate that dynamins are important, redundant regulators of DCV fusion, especially during prolonged stimulation. The fact that initial release was increased in dynamin 1 and 3 DKO and dynamin 1 single KO neurons suggests that dynamin 1 may have an additional inhibitory role during (initial) DCV exocytosis.

DCV exocytosis is enriched in synapses (*6*, *8*). To test whether the absence of SV endocytosis affects DCV exocytosis, the distance between single DCV fusion events and the synapse and between two fusion events was quantified, using synapsin-mCherry as a live synapse marker (Fig. 2I). In control, dynamin 3 KO, neurons, approximately 65% of DCV exocytosis occurred within 1 μm from a synapse, while in both dynamin 1 and 3 DKO and TKO, the average distance increased by >1 μm (Fig. 2I). In TKO neurons, the distance between individual DCV fusion events was larger, and the probability that multiple DCVs fused at the same location was 30% lower compared to both dynamin 3 KO and 1 and 3 DKO (Fig. 2J). Dynamin 1 or 2 expression alone was sufficient to restore a normal distance between fusion events (Fig. 3I). Hence, when dynamins 1 and 3 are absent and SV endocytosis is blocked, DCVs fuse less often in synapses. However, when all three dynamins are absent, DCVs are less likely to fuse at the same location, suggesting a unique role of dynamins in recovering DCV fusion sites.

To test whether DCVs fuse less often in synapses due to a reduced number of DCVs in synapses, we quantified NPY-SEP puncta overlapping with the synapse marker synaptophysin before and after stimulation using stimulated emission depletion (STED) microscopy (fig. S3H). No significant differences in the number of DCVs were detected between the genotypes and between unstimulated and stimulated conditions (fig. S3, I to K). This is in line with recent studies showing a normal DCV distribution while DCV fusion is severely inhibited (*6*, *17*).

The fluorescence intensity of single DCV fusion events, as indicator for DCV loading, was similar (fig. S2, H and J). The duration of individual DCV fusion events, mainly determined by fusion pore stability (*30*, *40*, *41*), was significantly increased in dynamin 1 and 3 DKO and TKO neurons (fig. S2, F and G) and in dynamin 1 KO neurons but not in other single dynamin KOs (fig. S2, H and I). Together, the data show that deletion of all dynamins strongly reduces DCV exocytosis via a putative defect in recovering of fusion sites, while leaving DCV biogenesis and cargo loading unaffected.

Dynamin acutely regulates DCV exocytosis

As an independent confirmation of the role of dynamins in DCV fusion and recovering of fusion sites, the chemical dynamin inhibitors dynasore (*42*) and dyngo-4a (*43*) were acutely applied to WT neurons. Both compounds inhibit the function of dynamin during its assembly into helixes; dynasore also inhibits dynamin during polymerization into rings (Fig. 4A) (*43*).

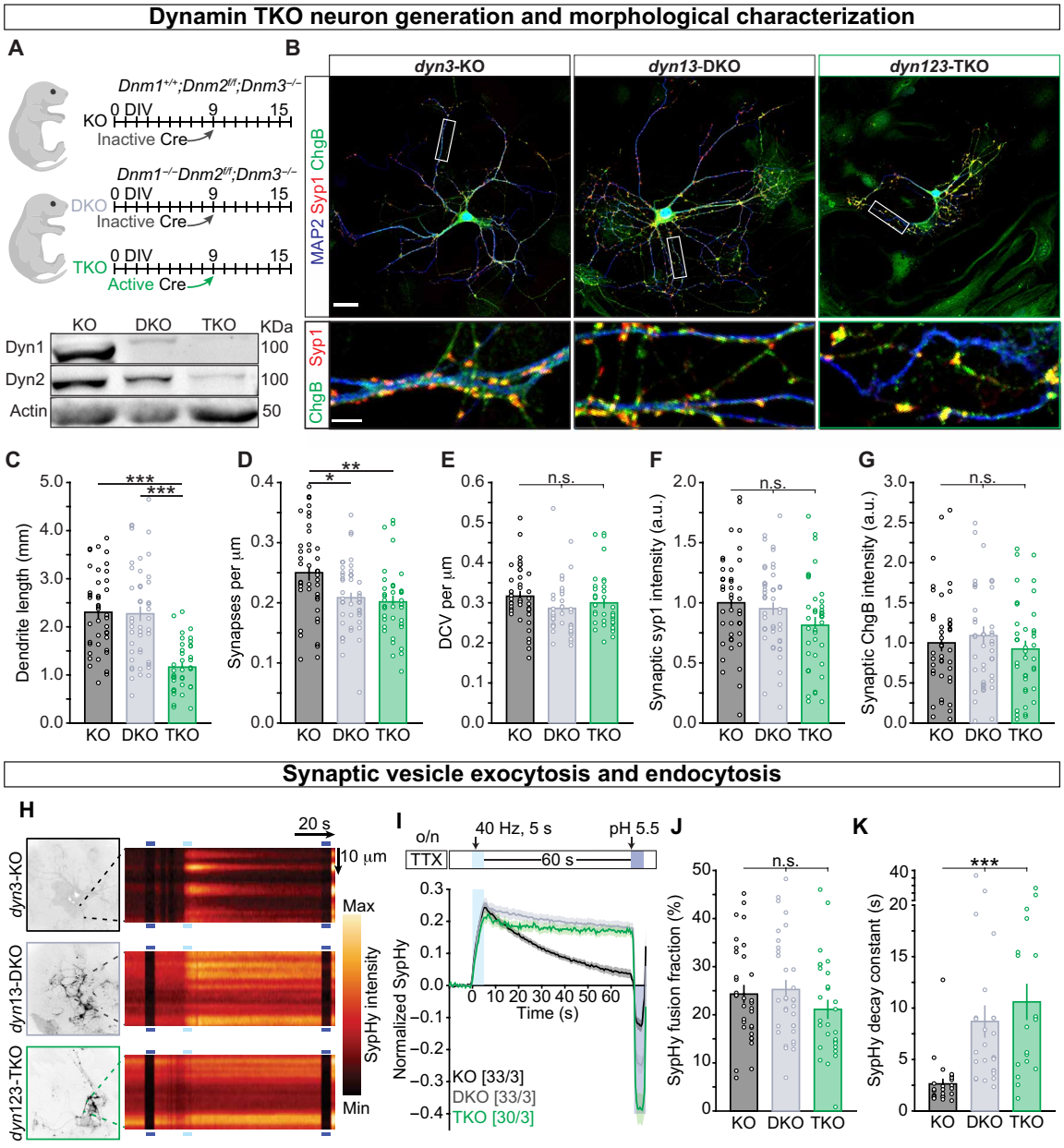

Fig. 1. Dynamins 1, 2, and 3 are required for normal dendritic length but dispensable for SV exocytosis. (**A**) Schematic representation of the experimental design. Neuronal cultures from *Dnm1*$^{-/-}$; *Dnm2*$^{lox/lox}$; *Dnm3*$^{-/-}$ pups were infected at DIV 9 with Cre recombinase to generate dynamin TKO neurons. Dynamin 3 KO littermate pups were used as control. Cultures were analyzed at DIV 15. Bottom: Typical Western blot showing the absence of dynamins 1 and 2 in DKO and TKO cultures. (**B**) Typical confocal images of isolated neurons immunostained for MAP2 (blue), synaptophysin 1 (SYP1, red), and the DCV marker chromogranin B (CHGB, green). Scale bars, 30 µm (top) and 10 µm (bottom). (**C**) Total dendritic length in millimeters. (**D**) Synapsin1-positive synapse density in MAP2-positive dendrites. (**E**) Chromogranin B–positive puncta density in MAP2-positive dendrites. (**F**) Synapsin1 immunoreactivity in synapses normalized to intensity in dynamin 3 KO neurons. (**G**) Chromogranin B immunoreactivity in synapses normalized to intensity in dynamin 3 KO neurons. (**H**) Typical neurons infected with the SV fusion marker SypHy (left), typical kymograph of a neurite showing SypHy intensity decrease upon pH 5.5 superfusion (purple bars), and the increase in intensity during electrical stimulation of 40 Hz for 5 s (light blue bars). Scale bar, 25 µm. (**I**) Top: Imaging protocol. Bottom: The average signal from active synapses, normalized from baseline to maximum fluorescence upon NH_4Cl superfusion. For visualization clarity, the first pH 5.5 superfusion and the NH_4Cl superfusion were excluded from the graph. (**J**) SV exocytosis expressed as the ratio of the maximum SypHy intensity during stimulation to the maximum during NH_4Cl stimulation. (**K**) SV endocytosis expressed as the SypHy signal decay time constant τ in the 60 s after field stimulation. Traces show means ± SEM (shaded area). Columns and dots represent individual litters and neurons, respectively. *$P < 0.05$; **$P < 0.01$; ***$P < 0.001$. n.s., not significant; a.u., arbitrary units.

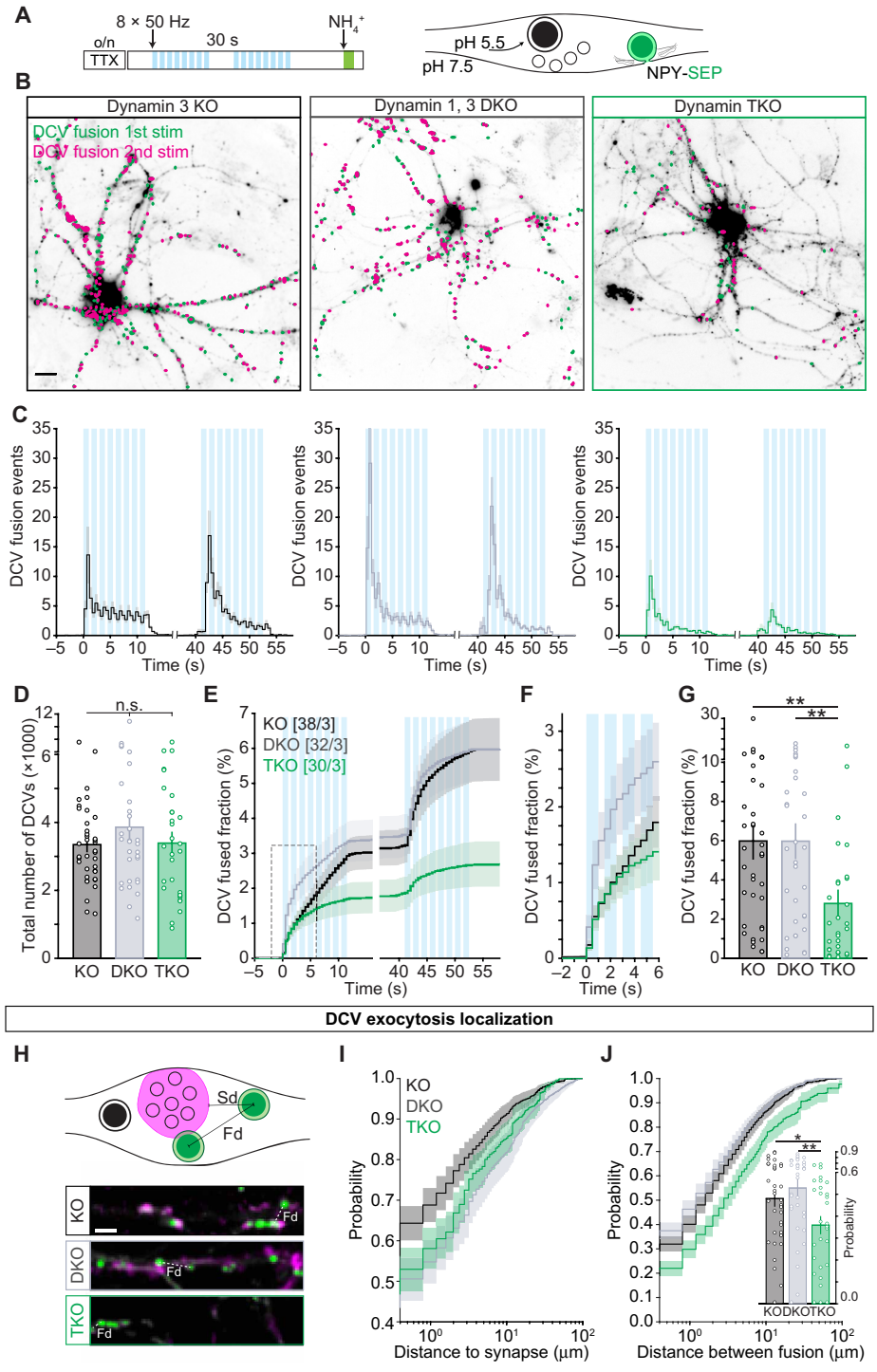

Fig. 2. Dynamin is a major regulator of DCV exocytosis. (**A**) Schematic representation of DCV fusion assay. DCVs are labeled with NPY-SEP, and neurons are stimulated with two trains of eight bursts of 50 APs at 50 Hz (light blue bars). (**B**) Representative neurons during NH_4Cl superfusion superimposed with NPY-SEP fusion events (green dots for the first stimulation and magenta for the second). Scale bar, 25 μm. (**C**) Histograms of the average number of DCV fusion events per cell during stimulation (light blue bars). (**D**) Total number of DCVs per cell quantified upon NH_4Cl superfusion. (**E**) Cumulative fraction of DCV fusion events during stimulation. The fraction is calculated as the number of DCVs fusing per frame divided by the total number of NPY-SEP puncta per neuron. (**F**) Zoom of the first four trains of 50 APs at 50 Hz. (**G**) Fraction of NPY-SEP–labeled DCV fusing during stimulation. (**H**) Schematic representation of the DCV fusion distance assay. Sd represents the distance between the center of an NPY-SEP fusion event and the closest pixel inside a synapsin-positive synapse. Fd represents the distance between the centers of two individual NPY-SEP fusion events. (**I**) Cumulative probability of a DCV fusion event in relation to distance from synapses in logarithmic scale. (**J**) Cumulative probability of a DCV fusion event in relation to distance from another DCV fusion event in logarithmic scale. Inset represents the probability of two fusion events being closer than 1.6 μm apart, indicating overlapping of the two regions. Traces show means ± SEM (shaded area). Columns and dots represent individual litters and neurons, respectively. *$P < 0.05$; **$P < 0.01$.

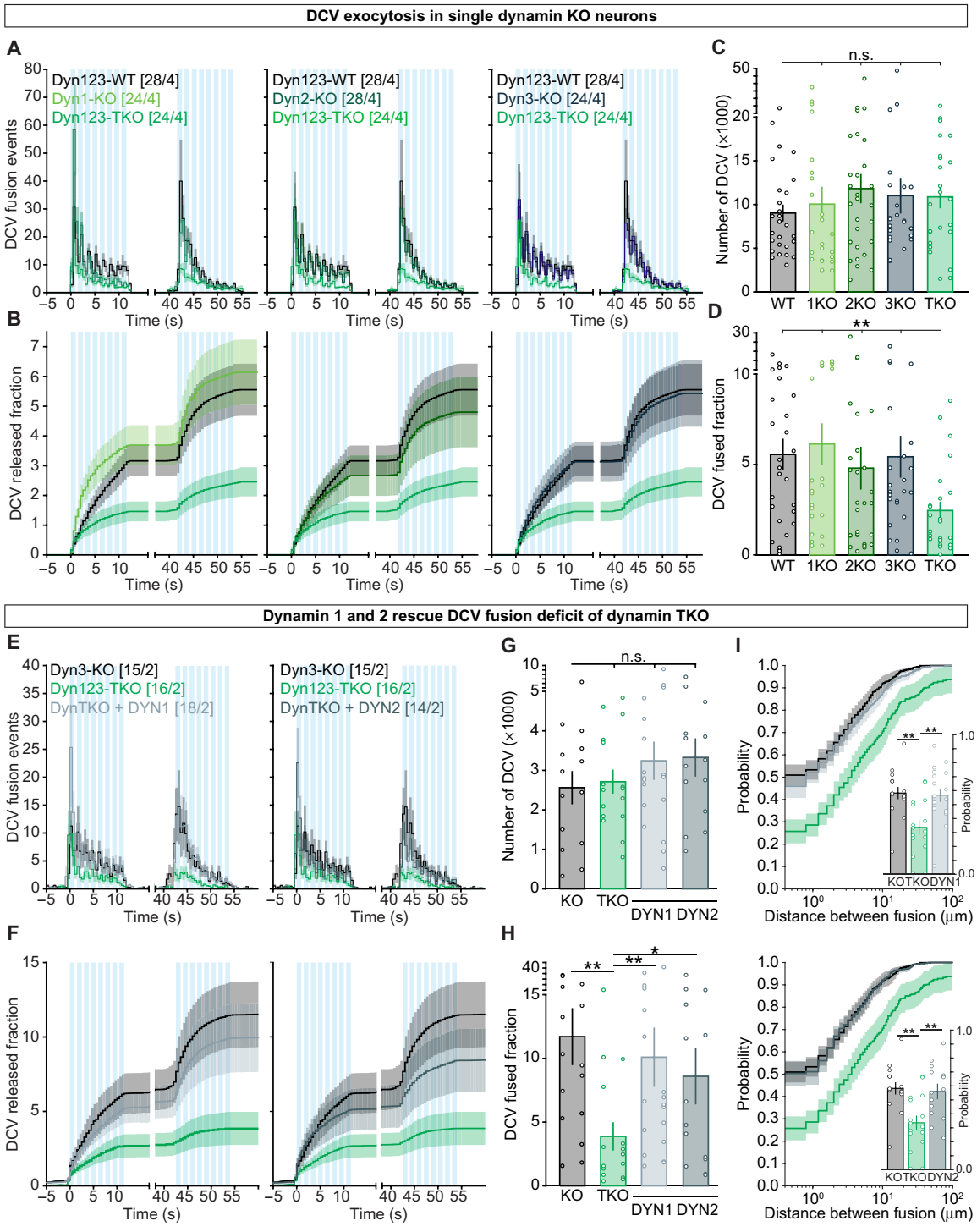

Fig. 3. Dynamins 1 and 2 have different roles in DCV exocytosis. (**A**) Histograms of the average number of DCV fusion events per cell during stimulation (light blue bars). (**B**) Cumulative fraction of DCV fusion events during stimulation. The fraction is calculated as the number of DCVs fusing per frame divided by the total number of NPY-SEP puncta per neuron. (**C**) Total number of DCVs per cell quantified upon NH_4Cl superfusion. (**D**) Fraction of NPY-SEP–labeled DCV fusing during stimulation. (**E**) Histograms of the average number of DCV fusion events per cell during stimulation (light blue bars). (**F**) Cumulative fraction of DCV fusion events during stimulation. The fraction is calculated as the number of DCVs fusing per frame divided by the total number of NPY-SEP puncta per neuron. (**G**) Total number of DCVs per cell quantified upon NH_4Cl superfusion. (**H**) Fraction of NPY-SEP–labeled DCV fusing during stimulation. (**I**) Cumulative probability of a DCV fusion event in relation to distance from another DCV fusion event in logarithmic scale. Inset represents the probability of two fusion events being closer than 1.6 μm apart, indicating overlapping of the two regions. Traces show means ± SEM (shaded area). Columns and dots represent individual litters and neurons, respectively. *$P < 0.05$; **$P < 0.01$.

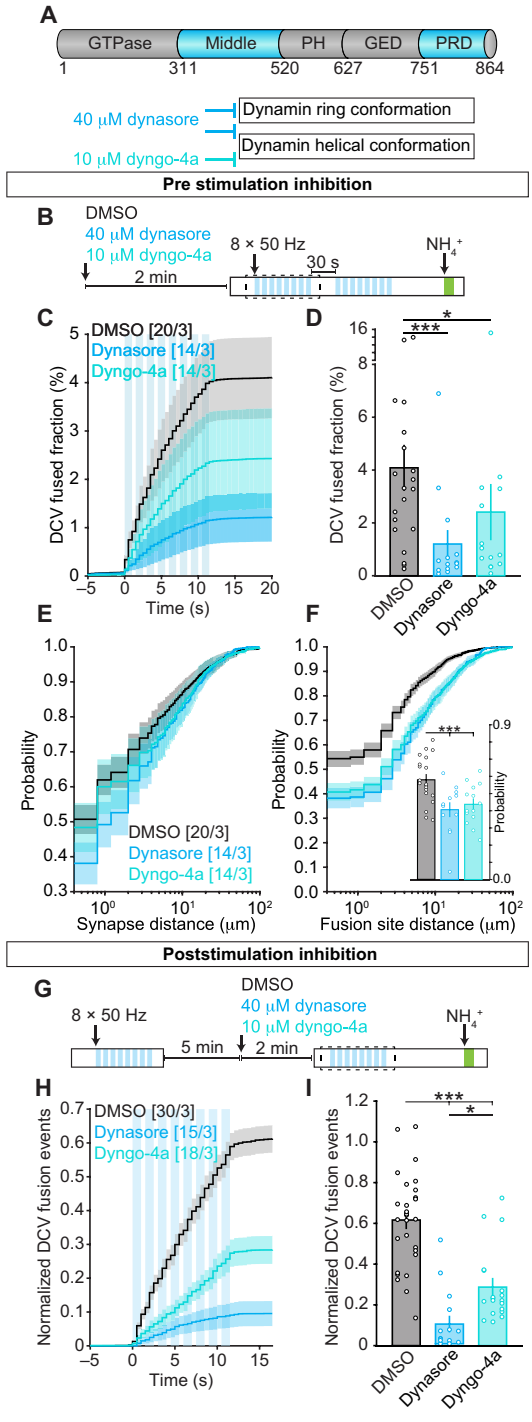

Fig. 4. Dynamin acutely regulates DCV exocytosis. (**A**) Schematic representation of the structure of dynamin. In light blue, the domains where dynasore and dyngo-4a are predicted to act to inhibit dynamin function. (**B**) Representation of the DCV fusion assay. Neurons were selected on the basis of morphology and the presence of NPY-SEP–labeled DCVs. Dynasore (40 μM) or 10 μM dyngo-4a was added to the imaging media and incubated for 2 min before stimulation (light blue bars). DMSO (1‰) was used as a control. (**C**) Cumulative fraction of DCV fusion events during stimulation. The fraction is calculated as the number of DCVs fusing per frame divided by the total number of NPY-SEP puncta per neuron. (**D**) Fraction of NPY-SEP–labeled DCV fusing during stimulation. (**E**) Cumulative probability of a DCV fusion event in relation to distance from synapses in logarithmic scale. (**F**) Cumulative probability of a DCV fusion event in relation to distance from other DCV fusion event in logarithmic scale. Inset represents the probability of two fusion events being closer than 1.6 μm apart, indicating overlapping of the two regions. (**G**) Representation of the inhibition protocol and DCV fusion assay. Dynasore (40 μM) or 10 μM dyngo-4a was added to the imaging media and incubated for 2 min before a second stimulation (light blue bars). DMSO (1‰) was used as a control. (**H**) Cumulative fraction of DCV fusion events during the second stimulation. The fraction is calculated as the number of DCV fusions per frame during the second stimulation divided by the total number of DCVs fusing during the first stimulation. (**I**) Fraction of NPY-SEP–labeled DCV fusing during the second stimulation. Traces show means ± SEM (shaded area). Columns and dots represent individual litters and neurons, respectively. *$P < 0.05$; ***$P < 0.001$.

WT neurons expressing NPY-SEP were incubated with inhibitors (40 and 10 μM for dynasore and dyngo-4a, respectively) 2 min before stimulation, and incubation with dimethyl sulfoxide (DMSO) was used as a control (Fig. 4B). These concentrations and incubation times were chosen to prevent dynamin-independent effects (*28*, *37*, *44*, *45*). Incubation of dynasore resulted in an ~80% inhibition of DCV exocytosis, while dyngo-4a resulted in a milder, 50%, reduction of DCV exocytosis (Fig. 4, C and D), especially during prolonged stimulation (fig. S4, D to F). Both compounds did not affect the distance of DCV exocytosis from synaptic sites (Fig. 4E). However, they both increased the distances between individual DCV fusion events and lowered the probability that multiple DCVs fused at the same location by approximately 30% (Fig. 4F). Hence, acute pharmacological inhibition of dynamins not only disrupts DCV exocytosis to a similar extent as gene inactivation of all three dynamin genes but also prevents DCVs from fusing at the same site.

The acute effect of dynamin inhibition also allowed for within-cell measurements in which we applied inhibitors for 2 min in between two bursts of eight trains of 50 APs at 50 Hz (Fig. 4G and fig. S4, A to C). This led to an even stronger inhibition of DCV fusion: 80% for dynasore and 70% for dyngo-4a (Fig. 4, H and I). The duration of single fusion events was significantly increased upon dyngo-4a incubation but not with dynasore (fig. S4, J and K). To test for dynamin-independent effects of the inhibitors (*37*), dynamin TKO neurons were incubated with 40 μM dynasore or 10 μM dyngo-4a (fig. S5). DCV exocytosis was not further decreased in these neurons (fig. S5F), indicating that the effect of dynasore and dyngo-4a on DCV exocytosis was due to the specific inhibition of dynamin. The differences observed between neurons treated with dynasore compared to dyngo-4a suggest that the two compounds modulate different functions of dynamin in DCV exocytosis. Together, genetic and pharmacological perturbations both indicate that dynamins promote DCV exocytosis and the likeliness that DCVs fuse at the same location and regulate the duration of individual fusion events.

Dynamin GTPase activity is required to support DCV exocytosis

Dynamin oligomerization stimulates its intrinsic GTPase activity (*46*). Since dynasore and dyngo-4a reduce DCV exocytosis in WT neurons, we investigated whether dynamin GTPase activity is required for efficient DCV exocytosis. To test this, dynamin TKO neurons were rescued with WT dynamin 2 or dynamin 2 with a point mutation in Lys^{44} (K44A), which abolishes guanosine triphosphate (GTP) binding and hydrolysis (Fig. 5A) (*47*, *48*). Expression of dynamin 2 WT in TKO neurons restored DCV fusion to the same levels as the control dynamin 3 KO neurons. In contrast, the K44A mutant failed to restore fusion (Fig. 5, C and E to G). Compared to dynamin 3 KO, TKO neurons rescued with dynamin 2 showed increased DCV exocytosis during the first four 50-AP trains, while dynamin 2 K44A reduced exocytosis even more than in TKO (Fig. 5, D and E). In addition, only dynamin 2 WT restored a normal average distance between DCV fusion sites and synapses (Fig. 5F), while expression of dynamin 2 K44A resulted in a marked increase in the distance between individual DCV fusion events (Fig. 5G), which can be explained by its dominant negative phenotype. Together, these data indicate that the GTPase activity of dynamin is essential to support DCV fusion and recovery of fusion sites. In addition, excess GTPase-deficient dynamin 2 functions as dominant negative for DCV fusion.

Dynamin regulates syntaxin-1B availability

The yeast dynamin ortholog Vps1 binds the syntaxin ortholog Vam3p to regulate vacuolar fusion (*20*, *22*). In chromaffin cells, dynamin coimmunoprecipitates with syntaxin-1 (*49*), and in rat synaptosomes, syntaxin-1B cross-links with the pleckstrin homology domain (PH domain) of dynamin (*50*). Therefore, we hypothesized that dynamin may promote DCV exocytosis and recovery of the same fusion sites by regulating syntaxin function or availability. To test this hypothesis, immunostaining with antibodies against syntaxin-1A and syntaxin-1B was used to assess syntaxin levels and distribution using synaptophysin as a synapse marker (Fig. 6, A to C). Syntaxin-1A fluorescence intensity was mildly but significantly decreased in both dynamin 1 and 3 DKO and TKO neurons (Fig. 6B). Syntaxin-1B fluorescence intensity was decreased in dynamin 1 and 3 DKO neurons to a similar extent as syntaxin-1A, but in dynamin TKO neurons, this reduction was pronounced (Fig. 6C). In WT neurons, dynamin inhibition with dynasore, but not dyngo-4a, showed a similar reduction in syntaxin-1B signal intensity (fig. S7, A and B). In contrast to immunocytochemistry, Western blot analysis showed that the total levels of syntaxin-1A, syntaxin-1B, and MUNC18-1 were not reduced (Fig. 6F), while the SNAP-25 and RAB3 levels were lower, as previously reported (Fig. 6G) (*27*). These data indicate that in the absence of dynamins, staining efficiency for syntaxin-1B, and to a lesser extent 1A, is reduced, suggesting that syntaxin-1B is especially less accessible for the antibody, probably due to multimerization, as shown before (*51*, *52*).

To resolve the distribution of syntaxin-1B at synapses and in proximity of DCVs with higher resolution, we performed STED microscopy on neurons infected with NPY-SEP and immunolabeled with syntaxin-1B and synaptophysin (Fig. 6D and fig. S7E). We confirmed that syntaxin-1B signal intensity was reduced (fig. S7, F to H) and also observed a small but significant reduction in intensity variation (fig. S7J) in TKO synapses, both before and after stimulation. Similarly, syntaxin-1B intensity was reduced in proximity of DCVs (Fig. 6E), and syntaxin-1B clusters were more abundant yet smaller (fig. S7, K and L) in TKO neurons compared to control neurons. Together, these data show that dynamin regulates syntaxin-1 availability both at synapses and at nonsynaptic locations without affecting the overall expression level.

Syntaxin-1 self-assembles in $PI(4,5)P_2$ (phosphatidylinositol 4,5-bisphosphate) clusters via its polybasic domain (*53*, *54*), resulting in reduced immuno-availability (*55*), as we observed in TKO neurons. Previous experiments showed that SNAP-25 can recruit syntaxin-1 from these clusters, thereby increasing syntaxin-1 immunoavailability (*51*). Given the fact that SNAP-25 levels are reduced in TKO neurons (Fig. 6G), we tested whether SNAP-25 overexpression restored a normal syntaxin-1B immunoreactivity in dynamin DKO and TKO neurons (fig. S7G). SNAP-25 overexpression increased syntaxin-1B immunoreactivity in dynamin 3 KO and dynamin 1 and 3 DKO neurons. However, in dynamin TKO neurons, SNAP-25 overexpression failed to increase syntaxin-1B immunoreactivity (fig. S7C). This suggests that SNAP-25–mediated syntaxin-1 recruitment requires dynamins.

A second explanation for the observed decrease in syntaxin-1B immunoreactivity is an enhanced recruitment into SNARE complexes (*56*, *57*). To test this, high-density dynamin 3 KO and TKO cultures were lysed in 2% SDS and run on SDS–polyacrylamide gel electrophoresis (PAGE) after 5 min at 100°C (to disrupt SNARE complexes) or room temperature (RT) (leaving SNARE complexes intact) (Fig. 6, H to K). We observed that syntaxin-1A was present in SNARE

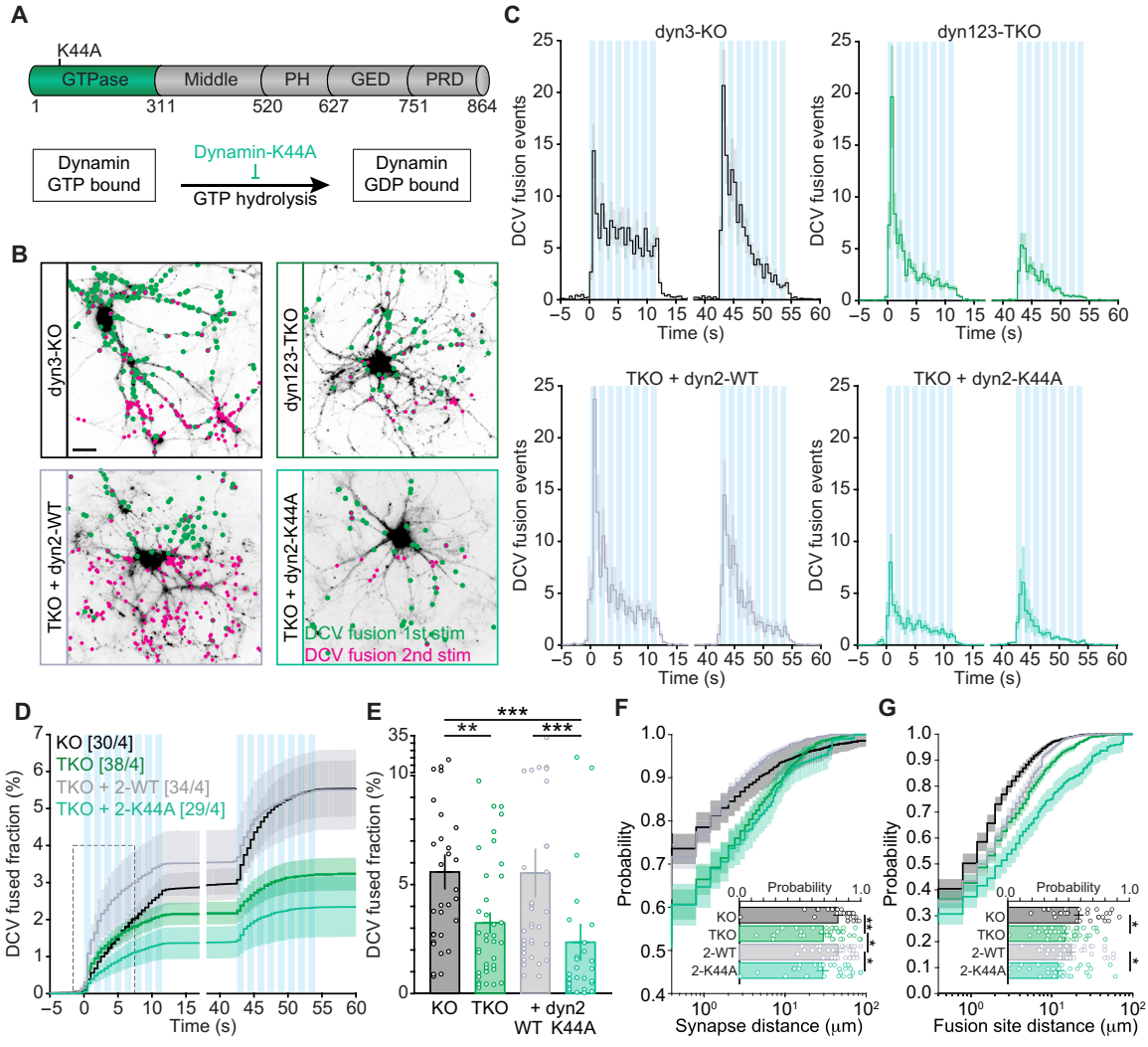

Fig. 5. Dynamin GTPase activity is required to support DCV exocytosis. (**A**) Schematic representation of the structure of dynamin. In green, the GTPase domain and the K44A point mutation. (**B**) Representative neurons during NH_4Cl superfusion superimposed with NPY-SEP fusion events (green dots for the first stimulation and magenta for the second). (**C**) Histograms of the average number of DCV fusion events per cell during stimulation (light blue bars). (**D**) Cumulative fraction of DCV fusion events during stimulation. The fraction is calculated as the number of DCVs fusing per frame divided by the total number of NPY-SEP puncta per neuron. (**E**) Fraction of NPY-SEP–labeled DCV fusing during stimulation. (**F**) Cumulative probability of a DCV fusion event in relation to distance from synapses in logarithmic scale. (**G**) Cumulative probability of a DCV fusion event in relation to distance from other DCV fusion event in logarithmic scale. Traces show means ± SEM (shaded area). Columns and dots represent individual litters and neurons, respectively. *$P < 0.05$; **$P < 0.01$; ***$P < 0.001$. Scale bar, 25 μm (B).

complexes at a similar level in TKO and 3KO neurons, while the presence of syntaxin-1B in SNARE complexes was reduced by ~50% in TKO neurons compared to dynamin 3KO (Fig. 6, I and K). Together, these data suggest that in the absence of dynamins, syntaxin-1B recruitment by SNAP-25 and integration into SNARE complexes are both impaired.

Dynamin is required downstream of αSNAP to regulate DCV exocytosis

The fully zippered *cis*-SNARE complexes, residing on the plasma membrane after SV fusion, are highly stable (*57*). Their disassembly requires NSF, which is recruited to the SNARE complex by αSNAP (*58*, *59*). In addition, αSNAP/NSF disassemble different types of SNARE complexes including fusogenic *trans*-SNARE (*60*, *61*) and syntaxin tetramers (*62*), a conformation that prevents the binding to SNAP-25 (*62*). To test whether the reduced syntaxin-1B immunoavailability is due to an increased propensity for the tetrameric conformation, αSNAP was transiently overexpressed in dynamin 3 KO and TKO neurons (Fig. 7A). Syntaxin-1B immunoreactivity in synaptophysin-positive synapses increased by 30% in TKO neurons, restoring levels to control (Fig. 7B and fig. S8, A to C). In TKO neurons rescued with dynamin 2 K44A, αSNAP did not rescue syntaxin-1B immuno-availability (Fig. 7B and fig. S8, A to C). We conclude that in dynamin TKO neurons, syntaxin-1B is present in a nonreceptive configuration that can be disassembled via αSNAP/NSF, but not SNAP-25, interaction.

Last, we tested whether transient αSNAP overexpression restores DCV fusion in dynamin TKO neurons (Fig. 7, C to F). In dynamin 3 KO neurons, but not in TKO neurons, αSNAP overexpression increased DCV exocytosis (Fig. 7F), in particular during the first

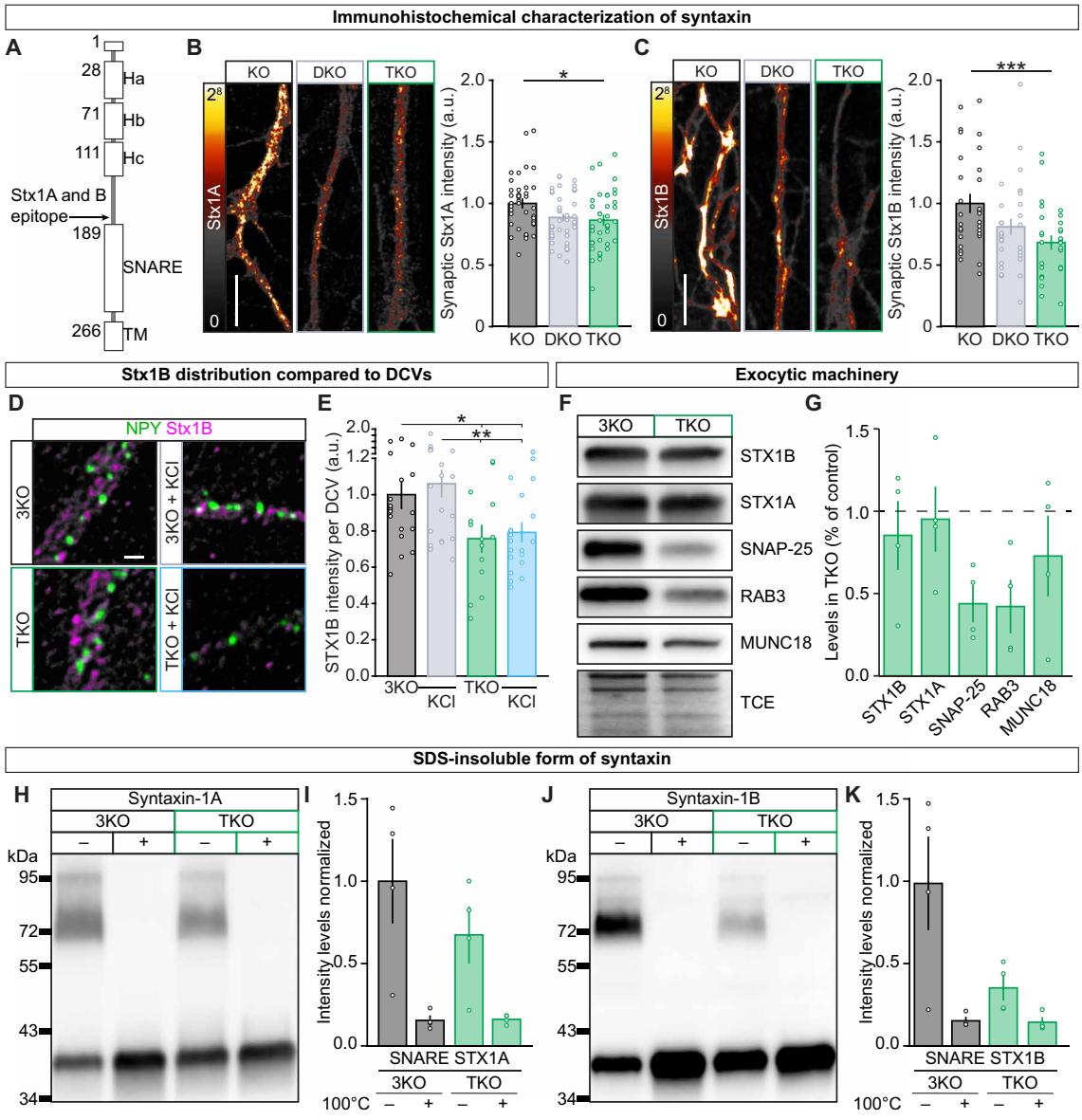

Fig. 6. Dynamin is required for syntaxin-1B assembly into SNARE complexes. (**A**) Schematic representation of the structure of syntaxin-1 with the indicated antibody epitope for both syntaxin-1A and syntaxin-1B. (**B**) Left: Representative neurites immunostained for syntaxin-1A. Right: Quantification of syntaxin-1A immunoreactivity in Syp1-positive synapses, normalized by the intensity in dyn3-KO neurons. (**C**) Left: Representative neurites immunostained for syntaxin-1B. Right: Quantification of syntaxin-1B immunoreactivity in Syp1-positive synapses, normalized by the intensity in dyn3-KO neurons. (**D**) Representative STED pictures of dynamin 3KO and TKO neurites with and without incubation with 50 mM KCl solution, labeled with NPY-SEP, and immunostained for syntaxin-1B. (**E**) Quantification of syntaxin-1B immunoreactivity at NPY-positive locations, normalized by the intensity of dynamin 3KO neurons. (**F**) Representative Western blot evaluation of exocytic proteins in dynamin 3 KO and TKO neuronal culture. (**G**) Quantification of protein levels in TKO normalized to 3KO cortical neuron culture. Measurements were made in four independent cultures. (**H**) Representative Western blot of SDS-resistant fraction of syntaxin-1A; samples were incubated with SDS and left either at RT (–) or at 100°C (+) for 10 min. (**I**) Quantification of syntaxin-1A levels in SDS-resistant SNARE complexes. Measurements were made in four independent cultures. (**J**) Representative Western blot of SDS-resistant fraction of syntaxin-1A; samples were incubated with SDS and left either at RT (–) or at 100°C (+) for 10 min. (**K**) Quantification of syntaxin-1A levels in SDS-resistant SNARE complexes. Measurements were made in four independent cultures. Columns and dots represent individual litters and neurons, respectively. *$P < 0.05$; **$P < 0.01$; ***$P < 0.001$. Scale bars, 25 μm (B and C) and 2 μm (D).

50-AP trains of the second stimulation (fig. S8I). Increased expression of αSNAP did not alter the distance from synapses in either genotype, while it reduced the distance between individual DCV fusion events in control, dynamin 3 KO neurons, while increasing the distance in TKO neurons (fig. S8, F and G). Thus, the data suggest that dynamin is required for DCV exocytosis downstream of αSNAP-mediated SNARE disassembly in mouse hippocampal neurons.

Disease-causing mutations of dynamin fail to support DCV exocytosis and syntaxin-1B availability

Dynamin binds to $PI(4,5)P_2$ at the plasma membrane via its PH domain (*63*, *64*). In addition to dynamin positioning, this interaction was reported to function in regulating dynamin GTPase activity (*65*). Multiple autosomal dominant disease-causing mutation of dynamin is present in the PH domain, predominantly in

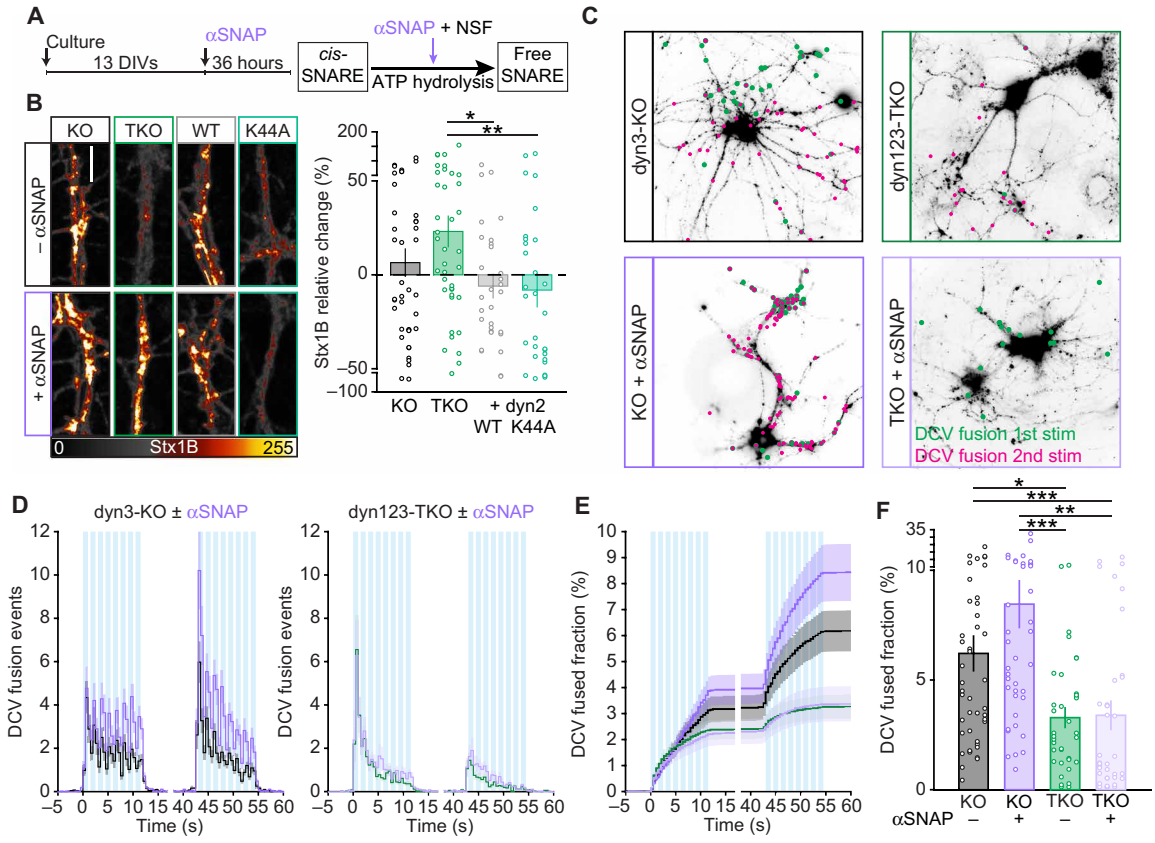

Fig. 7. Dynamin is required downstream of αSNAP to regulate DCV exocytosis. (**A**) Schematic representation of the experimental procedure. αSNAP was overexpressed for 36 hours before DCV fusion assay. Right: Representation of the mechanisms of action of αSNAP in resolving *cis*-SNARE complexes into individual proteins via NSF-dependent ATP hydrolysis. (**B**) Left: Representative naïve neurites (top) and neurites overexpressing αSNAP (bottom) immunostained for Stx1B. Scale bar, 25 μm. Right: Quantification of Stx1B immunoreactivity in syp1-positive synapses, normalized by the intensity in naïve synapses of the same genetic background. (**C**) Representative neurons during NH_4Cl superfusion superimposed with NPY-SEP fusion events (green dots for the first stimulation and magenta for the second). (**D**) Histograms of the average number of DCV fusion events per cell during stimulation (light blue bars). (**E**) Cumulative fraction of DCV fusion events during stimulation. The fraction is calculated as the number of DCVs fusing per frame divided by the total number of NPY-SEP puncta per neuron. (**F**) Fraction of NPY-SEP–labeled DCV fusing during stimulation. Traces show means ± SEM (shaded area). Columns and dots represent individual litters and neurons, respectively. *$P < 0.05$; **$P < 0.01$; ***$P < 0.001$.

Charcot-Marie-Tooth (CMT) disease and centronuclear myopathy (CNM) (*66*). To test whether the PH domain of dynamin is required to support DCV exocytosis, we introduced several CMT/CNM mutations in TKO neurons (Fig. 8, A and B).

First, neuronal cultures were incubated with transferrin coupled to Alexa Fluor 488 (Trf-488; Fig. 8C), to assess whether any of the mutation was able to support endocytosis. None of the mutants rescued Trf-488 endocytosis to the same level as the control dynamin 3 KO neurons (Fig. 8C). We then tested whether any of these mutations were able to restore syntaxin-1B immuno-availability (Fig. 8D). As for their endocytosis capacity, none of the tested mutants restored the signal intensity of syntaxin-1B to the level of dynamin 3 KO or TKO expressing dynamin 2 WT (Fig. 8D). Thus, despite reports of increased membrane fission capacity of several CNM-associated mutants in artificial fission assays (*67*), the nine mutations tested here showed that the PH domain of dynamin is required to support constitutive transferrin endocytosis and syntaxin-1B accessibility.

We observed that the CNM-associated E560K mutant that was suggested to increase the binding affinity of dynamin for $PI(4,5)P_2$ (*67*, *68*) showed the lowest levels of syntaxin-1B immunoreactivity. Therefore, we used this mutant to test the role of $PI(4,5)P_2$ binding of dynamin in DCV exocytosis (Fig. 8E). Expression of dynamin 2 E560K restored neither DCV exocytosis in TKO neurons (Fig. 8, F to H) nor the distance between individual DCV fusion events (Fig. 8I). Together, these data provide evidence that disease-causing mutations, which reside in the PH domain of dynamin, are unable to promote syntaxin-1B accessibility. Thus, the dynamin-$PI(4,5)P_2$ interaction is required for its regulation of DCV exocytosis and recovery of fusion sites.

DISCUSSION

In this study, we investigated the function of the Vps1 orthologs dynamins 1 to 3 in neuromodulator exocytosis in mouse central nervous system (CNS) neurons. Dynamin TKO neurons, as well as WT neurons treated with the dynamin inhibitor dynasore or dyngo-4a, showed >50% reduction in DCV exocytosis during prolonged stimulation (Figs. 2 and 4), and the proportion of DCVs that fused at similar locations was reduced in TKO neurons (Fig. 2J). The expression of WT dynamin 2, but not GTPase (Fig. 5) or PH (Fig. 8) mutants in TKO neurons, restored DCV exocytosis. Last, in dynamin TKO neurons, syntaxin-1B was expressed at a normal level but in a

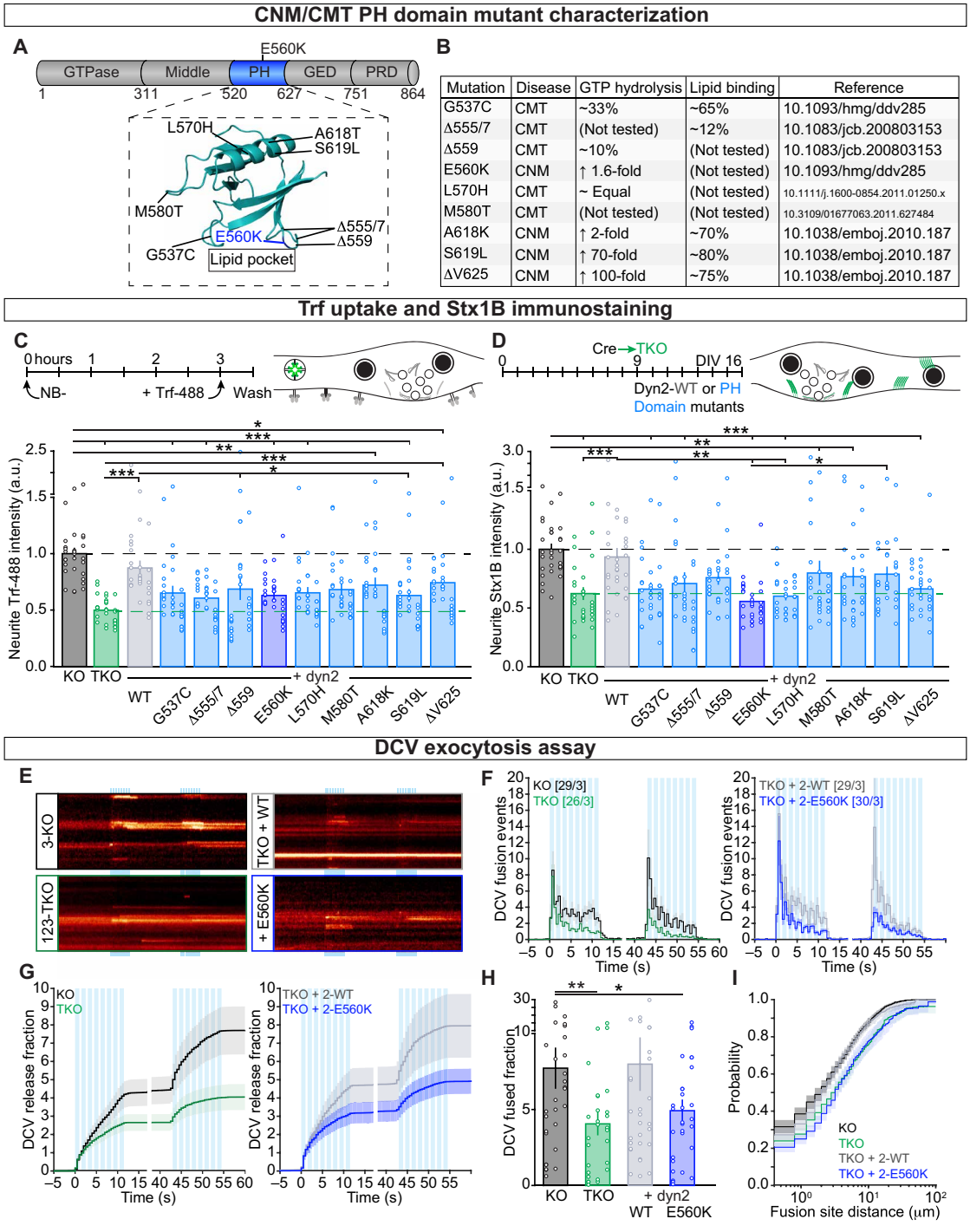

Mutation	Disease	GTP hydrolysis	Lipid binding	Reference
G537C	CMT	~33%	~65%	10.1093/hmg/ddv285
Δ555/7	CMT	(Not tested)	~12%	10.1083/jcb.200803153
Δ559	CMT	~10%	(Not tested)	10.1083/jcb.200803153
E560K	CNM	↑ 1.6-fold	(Not tested)	10.1093/hmg/ddv285
L570H	CMT	~ Equal	(Not tested)	10.1111/j.1600-0854.2011.01250.x
M580T	CMT	(Not tested)	(Not tested)	10.3109/01677063.2011.627484
A618K	CNM	↑ 2-fold	~70%	10.1038/emboj.2010.187
S619L	CNM	↑ 70-fold	~80%	10.1038/emboj.2010.187
ΔV625	CNM	↑ 100-fold	~75%	10.1038/emboj.2010.187

Fig. 8. CMT- and CNM-causing mutation of dynamin does not support DCV exocytosis. (**A**) Schematic representation of the structure of dynamin. In blue highlight is the PH domain and the E560K point mutation. Bottom: The crystal structure of the PH domain (PDB 1DYN) indicating nine mutations responsible for CMT diseases or CNM. (**B**) Table representing the mutated residues, the disease where it was found, the reported rate of GTP hydrolysis if tested, the lipid binding affinity if tested, and the reference for the characterization of the mutation properties. (**C**) Top: Schematic representation of the transferrin endocytosis assay. Cultures were starved in Neurobasal without B27 (NB-) for 3 hours and then incubated for 30 min with transferrin conjugated with Alexa-488 (Trf-488). Bottom: Quantification of Trf-488 intensity in neurites normalized by the intensity in dyn3-KO neurons. (**D**) Top: Schematic representation of the experimental procedure. Bottom: Quantification of Stx1B in neurites normalized by the intensity in dyn3-KO neurons. (**E**) Kymographs of NPY-SEP fusion events. Individual DCV fusion events, yellow dots in the images, were quantified semiautomatically. (**F**) Histograms of the average number of DCV fusion events per cell during stimulation (light blue bars). (**G**) Cumulative fraction of DCV fusion events during stimulation. The fraction is calculated as the number of DCVs fusing per frame divided by the total number of NPY-SEP puncta per neuron. (**H**) Fraction of NPY-SEP–labeled DCV fusing during stimulation. (**I**) Cumulative probability of a DCV fusion event in relation to distance from other DCV fusion event in logarithmic scale. Traces show means ± SEM (shaded area). Columns and dots represent individual litters and neurons, respectively. **P* < 0.05; ***P* < 0.01; ****P* < 0.001.

conformation inaccessible to antibody binding (Fig. 6A). A normal antibody accessibility was restored by αSNAP expression (Fig. 7A). We propose that dynamin promotes the organization of DCV fusion sites, downstream of αSNAP-mediated SNARE disassembly, by regulating the equilibrium between fusogenic and non-fusogenic syntaxin-1.

The role of dynamins in DCV exocytosis is distinct from known dynamin functions

Starting 6 days after Cre infection, dynamin TKO neurons were gradually lost (fig. S1B), suggesting that neurons require a minimal level of dynamin expression for survival (*37*). At least four observations suggest that our conclusions on dynamin's role in DCV exocytosis are not confounded by impaired cell viability: At the exact time when DCV exocytosis was found to be severely impaired, (i) SV exocytosis was unaffected in the same (Cre-infected TKO) neurons (Fig. 1, H to K, and fig. S1, F to L), as well as (ii) Ca^{2+} homeostasis, including a rapid decay after peak Ca^{2+} increases (fig. S1, C to E), and (iii) adenosine triphosphate (ATP)–dependent DCV trafficking and DCV distribution along the neurite arbor (Fig. 1, D to G). Moreover, (iv) acute inhibition of dynamin with two different compounds (Fig. 4 and fig. S4) impaired DCV exocytosis to a similar extent.

The role of dynamin in DCV exocytosis is also distinct from its well-established role in membrane fission and endocytosis (*25*, *29*, *37*, *46*, *47*, *69*). First, while endocytosis was fully blocked in dynamin 1 and 3 DKO neurons (Fig. 1, I and K), as previously shown (*26*–*28*, *70*), DCV exocytosis was normal (Fig. 2, A to G) and only impaired when all three dynamin genes were inactivated. Second, DCVs are produced by budding off from the trans-Golgi network, for which dynamins are dispensable (Fig. 2D), and do not depend on endocytosis. One aspect where dynamin-dependent membrane fission is relevant for DCV exocytosis is to restrict fusion pore opening during fusion events, as proposed for secretion in PC12 and chromaffin cells (*30*, *40*, *41*, *44*, *71*). However, a role in fusion pore restriction would lead to an increase, not to the observed decrease, in neuromodulator release in the absence of dynamins. The observed increase in individual fusion event duration in TKO neurons (figs. S2 and S4) confirms the role of dynamin-dependent fusion pore restriction also for neuronal DCV exocytosis. Together, our data suggest that dynamins have a unique, not previously characterized function in DCV exocytosis, distinct from their role in cell survival and well-characterized role in membrane fission and endocytosis.

Dynamins 1 and 2 support DCV exocytosis to a different extent

This study revealed several functional differences between different dynamin genes. First, we confirmed previous conclusions that SV endocytosis depends on dynamins 1 and 3, while dynamin 2 has only a marginal function (Fig. 1, H to K) (*26*, *27*, *70*). Second, the duration of individual DCV fusion events was longer in dynamin 1 KO and dynamin TKO neurons (fig. S2, F and L). Hence, on top of its (positive) role in promoting DCV exocytosis, dynamin 1, but not dynamin 2, limits DCV fusion duration, probably by promoting the fission of fusing DCVs and limiting cargo release, as previously proposed (*30*, *41*, *71*). Third, dynamin 1 and 3 DKO and dynamin 1 KO neurons showed a twofold increased DCV exocytosis during the initial phase of the stimulation (Figs. 2 and 3). A similar increase was also observed in dynamin TKO neurons expressing dynamin 2 WT (Figs. 5 and 8). Conversely, dynamin 2 single KO neurons show a tendency toward reduced DCV exocytosis during prolonged stimulation (Fig. 3). Hence, dynamin 2 expression is associated with higher DCV exocytosis and dynamin 1 with lower. However, both support DCV exocytosis, because overall inhibition of DCV exocytosis was only observed when all three dynamin genes were inactivated, and because expression of either dynamin 1 or 2 restored normal DCV fusion in dynamin TKO neurons. Given the conclusion that dynamin 1, but not dynamin 2, restricts the fusion pore (see above), the most likely scenario is that all dynamins support DCV exocytosis and that, on top of this, dynamin 1 selectively adds a layer of negative regulation, restricting the fusion pore.

Dynamins acutely promote DCV exocytosis and repeated use of fusion sites

Dynamin 2 K44A, which cannot bind and hydrolyze GTP (*48*), and the CNM-causing E560K mutation, which affects $PI(4,5)P_2$ binding (*67*), both did not support DCV exocytosis (Figs. 5 and 8). Furthermore, short (2-min) incubations with dynasore or dyngo-4a (Fig. 4) reduced DCV exocytosis to a similar extent as genetic perturbations. Known dynamin-independent effects of both compounds (*37*) were excluded (fig. S5). Therefore, we conclude that dynamins regulate DCV exocytosis via a direct (acute) action, requiring its GTPase function and $PI(4,5)P_2$ binding at the site of fusion, largely analogous to Vps1p function in yeast, where GTP hydrolysis acutely promotes vacuolar SNARE complex formation and fusion (*20*).

In mammalian CNS neurons, DCV exocytosis requires high-frequency stimulation (*6*, *8*, *72*–*74*). The initial phase of DCV exocytosis during high-frequency stimulation was unaltered in the absence of all three dynamins but severely inhibited subsequently (Fig. 2, F and G). This is in line with previous data from insulin-secreting β cells (*31*, *32*), where insulin secretion is initially normal but reduced later in the absence of dynamin 2. Thus, in naïve neurons, dynamin is not essential for DCV exocytosis but becomes severely rate-limiting during high-frequency stimulation.

The probability that DCVs fused at the same location was reduced (Figs. 2J inset and 4F inset). This suggests that dynamins regulate the recovery or reactivation of fusion sites after a previous fusion event. However, defective recovery/reactivation is insufficient to explain the total reduction in DCV exocytosis (compare effect sizes in Fig. 2, G and J). This suggests that dynamins have two crucial roles in DCV exocytosis: They acutely organize DCV fusion sites and, in addition, recover or reactivate fusion sites for repeated use. Besides, dynamin 1 has a third role in restricting the fusion pore (see above). Dynamin-independent processes, e.g., the actions of the MUNC13-RIM1-RAB3 complex, essential for DCV fusion (*17*), may compensate for dynamin deficiency under resting conditions and produce a normal initial number of fusion sites and a normal initial phase of DCV exocytosis. However, during prolonged stimulation, required for efficient DCV fusion, dynamin becomes severely rate-limiting both for first-time and repeated-use fusion sites.

Dynamin promotes DCV exocytosis by regulating syntaxin availability to drive fusion

In yeast, the dynamin homolog Vps1p directly binds the syntaxin homolog Vam3p to promote vacuolar fusion (*20*–*22*). An equivalent interaction between dynamin and syntaxin-1 was shown in bovine chromaffin cells (*49*) and rat synaptosomes (*50*), suggesting a conserved role for dynamin in binding to exocytic SNAREs. In the absence of dynamins, the accessibility of syntaxin-1B for its antibody was impaired (Fig. 6), although the total amount of protein was

normal (Fig. 6G). This suggests that syntaxin-1B is distributed in a different way in the absence of dynamin, providing less access for the antibody, as suggested before for reduced syntaxin-1 staining in the absence of another syntaxin interactor, SNAP-25 (*51*), and in analogy to yeast, where Vps1p clusters Vam3p (*22*). This idea is independently supported by our biochemical analyses showing that the proportion of syntaxin-1 in SNARE complexes and migrating on gel as monomers were both altered too (fig. S7K). Syntaxin-1 is known to exist in the cell as monomers and dimers with MUNC18-1 or SNAP-25 in *cis*-SNARE complexes and as tetramers (*53*, *75*, *76*). In this latter configuration, syntaxin-1 does not bind SNAP-25 (*62*) and is therefore considered non-fusogenic, similar to *cis*-SNARE complexes. Therefore, it seems plausible that dynamins regulate the equilibrium between such configurations, promoting a fusogenic and antibody-accessible state of syntaxin-1 (Fig. 6). Despite the high similarity and redundancy between the two proteins (*77*), dynamins regulate syntaxin-1B availability substantially more than syntaxin-1A availability, and the former appears to be more relevant for DCV fusion.

The non-fusogenic *cis*-SNARE complexes and syntaxin tetramers can both be disassembled by αSNAP/NSF [reviewed in (*78*, *79*)]. In yeast, Vps1 promotes Vam3-dependent vacuole fusion downstream of the action of αSNAP/NFS orthologs Sec17/18 (*cis*-SNARE disassembly) and recruits the HOPS complex to stabilize a fusogenic configuration and promote fusion (*20*, *21*, *58*, *80*). Because transient overexpression of αSNAP in dynamin TKO neurons restored syntaxin-1 accessibility, but not DCV fusion (Fig. 7), we conclude that a similar scenario applies to DCV exocytosis and that dynamin acts downstream of αSNAP/NSF-mediated *cis*-SNARE disassembly.

Together, we propose that, in addition to its fission role in endocytosis, dynamins promote the organization and recovery of DCV fusion sites, downstream of αSNAP-mediated SNARE disassembly, by acutely regulating the equilibrium between fusogenic and non-fusogenic syntaxin at DCV fusion sites in a GTPase-dependent manner. This role of dynamin-like GTPases in membrane fusion is evolutionarily conserved from yeast to regulated secretion in mammalian neurons.

MATERIALS AND METHODS

Laboratory animals and primary neuron cultures

All animals were housed and bred according to institutional and Dutch Animal Ethical Committee regulations (DEC-FGA 11-03). The generation of *Dnm1*$^{+/-}$; *Dnm2*$^{lox/lox}$; *Dnm3*$^{+/-}$ mice was previously described (*26*, *27*, *37*). Embryonic day 18 pups were humanely euthanized, and hippocampi were dissected in Hanks' balanced salt solution (Sigma-Aldrich) with 10 mM Hepes (Life Technology), digested in 0.025% trypsin (Life Technologies) for 20 min at 37°C, and dissociated with fire-polished Pasteur pipettes. Dissociated neurons were resuspended in Neurobasal supplemented with 2% B-27, 18 mM Hepes, 0.25% Glutamax, and 0.1% penicillin/streptomycin (Life Technologies) and plated at a density of 1300 neurons per well on astrocyte micro-island (*8*, *15*, *81*) in 12-well plates; for high-density cultures, 25,000 neurons per well were plated on pregrown glia cells. Astrocyte micro-islands were generated by plating 6000 rat glial cells per agarose-coated 18-mm glass coverslip, stamped with poly-D-lysine (0.1 mg/ml; Sigma-Aldrich) and rat tail collagen (0.7 mg/ml; BD Biosciences) (*82*). For Western blots and quantitative reverse transcription polymerase chain reaction, neurons were plated at a density of 250,000 neurons per well on plates coated with a solution of 0.0005% poly-L-ornithine and laminin (2.5 μg/ml) (Sigma-Aldrich). Neuronal cultures were kept in supplemented Neurobasal at 37°C and 5% CO_2 until DIV 15 to 16.

Plasmid and lentiviral infection

Dynamin 2 WT was extract from a complementary DNA library with primers forward 5′-CTACCGGACTCAGATCTCGAATGGGCAACCGCGGGATGG-3′ and reverse 5′-GTACCGTCGACTGCAGAATTCTAGTCGAGCAGGGACGGC-3′ and cloned into the plasmids pSyn(pr)Dynamin2-IRES2-NLSmCherry, pSyn(pr)Dynamin2(K44A)-IRES2-NLSmCherry, and pSyn(pr)Dynamin2(E560K)-IRES2-NLSmCherry. pSyn(pr)Synapsin-mCherry, pSyn(pr)NPY-pHluorin, pSyn(pr)BDNF-pHluorin, pSyn(pr)iCre-eGFP, and pSyn(pr)SNAP25-IRES2-eGFP were previously described (*6*–*8*, *15*, *17*, *39*). pSyn(pr)αSNAP-IRES2-NLSmCherry and pSyn(pr)NSF-IRES2-eGFP were made by substituting the cytomegalovirus promoter with synapsin promoter in plasmids previously described (*61*). All plasmids were sequenced-verified and subcloned into lentiviral vectors to produce viral particles (*83*).

Neuronal cultures were infected with Cre recombinase 9 DIVs after plating to generate dynamin TKO, and an inactive Cre (*84*) was used as a control for dynamin 1 and 3 DKO and dynamin 3 KO cultures. Rescue plasmids were added to the same mix. For all experiments, viruses encoding the protein of interest were added to the neuronal culture 6 days before the readout, and proper concentration of viruses were tested in WT cultures. For transient overexpression of αSNAP and NSF, neurons were infected with the appropriate concentration of viruses 36 hours before experiment.

Live-cell imaging

Neurons at DIV 14 to 15 were treated with tetrodotoxin (TTX; Sigma-Aldrich, 10 μM) overnight and then placed in the imaging chamber containing Tyrode's solution [2 mM $CaCl_2$, 2.5 mM KCl, 119 mM NaCl, 2 mM $MgCl_2$, 30 mM glucose, and 25 mM Hepes (pH 7.4)]. Following procedures previously described in (*39*), experiments were performed at RT with superfusion of Tyrode's buffer unless otherwise specified. Images were acquired on an Axiovert II microscope (Zeiss, Oberkochen, Germany) with a 40× oil objective [numerical aperture (NA) = 1.3] for SV fusion, DCV fusion, and trafficking or on a Nikon Eclipse Ti microscope with 63× oil objective (NA = 1.4) for axonal targeting. Time-lapse recordings were acquired using Metamorph 6 and an EM-CCD camera or using NIS-Elements 4.30 software. The acquisition frequency was 2 Hz for pHluorin-based assays and 1 Hz for trafficking and targeting assays.

For SypHy experiments, the imaging protocol included 10 s of baseline recording, 5 s of acid wash in Tyrode's solution [2 mM $CaCl_2$, 2.5 mM KCl, 119 mM NaCl, 2 mM $MgCl_2$, 30 mM glucose, and 25 mM MES (pH 5.5)], and allowed to recover for 15 s. As previously described (*39*), electrical field stimulation was then applied using a A-385 stimulus isolator (WPI) controlled by a Master 8 (AMPI), delivering 1-ms 30-mA pulses for 5 s at 40 Hz, followed by 1 min of recovery time, an additional 5 s of Tyrode's (pH 5.5) superfusion, and a final 5-s perfusion with modified Tyrode's solution containing NH_4Cl [2 mM $CaCl_2$, 2.5 mM KCl, 119 mM NaCl, 2 mM $MgCl_2$, 30 mM glucose, 25 mM Hepes, and 50 mM NH_4Cl (pH 7.4)] delivered by gravity flow through a capillary placed above the cell.

For DCV fusion, neurons were imaged for 30 s as baseline, stimulated with electrical field stimulation for eight pulses of 1 s at 50 Hz separated by 0.5 s, allowed to rest for 30 s after which the stimulation was repeated. After an additional 30 s of recovery, Tyrode's solution containing NH_4Cl was superfused for 5 s, as previously described (*39*).

For dynasore (40 μM; Merck Millipore) and dyngo-4a (10 μM; Abcam) experiments, stock solution were made in DMSO (Sigma-Aldrich) at 40 and 10 mM, respectively, as stored at −20°C. During image acquisition, aliquots were thawed and diluted 1:1000 in Tyrodes's (pH 7.4) solution, leading to a final DMSO concentration of 1 per mil (‰). For prestimulation inhibition protocols, neurons were identified on the basis of morphological appearance and presence of labeled synapses, and 40 μM dynasore, 10 μM dyngo-4a, or 1‰ DMSO was added to the coverslip and allowed to rest for 1.5 min before the start of the DCV fusion protocol described above. For poststimulation inhibition experiments, naïve neurons were recorded for 10 s of baseline, stimulated with electrical field stimulation for eight pulses of 1 s at 50 Hz separated by 0.5 s, and recorded for an additional 20 s. The recordings were then briefly analyzed for the presence of DCV fusion, within 5 min after stimulation. If the recording resulted positive for DCV fusion, 40 μM dynasore, 10 μM dyngo-4a, or 1‰ DMSO was added to the coverslip and allowed to rest for 1.9 min before the start of the new recording.

Immunostaining and STED and confocal microscopy

Neurons were fixed at DIV 15 to 16 with 3.7% formaldehyde (Merck) in phosphate-buffered saline [PBS; 137 mM NaCl, 2.7 mM KCl, 10 mM sodium phosphate buffer, 1.8 mM KH2PO4 (pH 7.4)] for 20 min. Cells were permeabilized in 0.5% Triton X-100 (Fisher Chemical) for 5 min and blocked with 0.1% Triton X-100 and 2% normal goat serum for 60 min. Primary antibody incubation with MAP2 (1:1000; Abcam), SMI312 (1:1000; BioLegend), synaptophysin 1, syntaxin-1A (1:500; SySy), syntaxin1B (1:500; SySy), and ChgB (1:500; SySy) was performed for 2 hours at RT. Alexa Fluor–conjugated secondary antibodies (1:1000; Invitrogen) were incubated for 1 hour at RT. For STED experiment, before fixation, a subset of neurons was stimulated for 5 min in a 50 mM KCl Tyrode's solution [2 mM $CaCl_2$, 50 mM KCl, 119 mM NaCl, 2 mM $MgCl_2$, 30 mM glucose, 25 mM Hepes (pH 7.4)], while another was incubated in regular Tyrode's solution. Incubation with primary antibody synaptophysin-1 (1:100) and syntaxin-1B (1:100) was performed for 2 hours at RT. Alexa Fluor 647 (1:100) and Abberior STAR-580 (1:100) were used as secondary antibody. Coverslips were mounted in Mowiol and imaged on a Nikon Eclipse Ti microscope confocal laser scanning microscope (40× objective; NA 1.3) with NIS-Elements 4.30 software. Images were acquired as Z-stack of three planes 250 μm apart and four images per plane with 15% overlap to ensure that the entire micro-island was in the field of view. STED microscopy was performed on a Leica TCS SP8 STED 3X microscope (Leica Microsystems, Wetzlar, Germany). Samples were illuminated at wavelengths of 499, 590, and 640 nm and depleted at 590 and 750 nm, respectively, for NPY-pHluorin, syntaxin-1B STAR-580, and synaptophysin Alexa-647. The signal was detected using a gated Hybrid Detector (HyD, Leica Microsystems) in photon-counting mode. STED images were acquired using a dedicated oil objective with ×100 magnification and NA of 1.4 (Leica Microsystems). A Z-stack was made with a step size of 150 nm and pixel size of 20 nm by 20 nm, optimized using Nyquist Calculator from SVI (Scientific Volume Imaging, Hilversum, The Netherlands). Last, deconvolution was performed with Huygens Professional (SVI).

Western blot

Cortical neurons were lysed at DIV 15 to 16. Lysates were run on an 8 to 15% gradient gel (Bio-Rad) for SDS-PAGE and transferred to a polyvinylidene difluoride membrane (Bio-Rad). Membranes were blocked with 5% milk (Merck) in PBS with 0.1% Tween 20 for 1 hour at RT and incubated in primary antibody against dynamin 1 and dynamin 2. For the *cis*-SNARE quantification, samples were collected on ice-cold lysis buffer, and one fraction was then heated at 100°C for 10 min, while another remained at RT as previously described (*56*, *57*). Membranes were incubated with primary antibody against Stx1A/B (HPC1; 1:1000; Abcam), Stx1B (1:1000; SySy), and actin (1:10,000; Chemicon) overnight at 4°C. Secondary alkaline phosphatase–conjugated antibodies (1:10,000; Jackson ImmunoResearch) were incubated for 30 min at RT. Membranes were visualized with AttoPhos (Promega) and scanned with a FLA-5000 fluorescent image analyzer (Fujifilm).

Image analysis

For SV fusion analysis, individual synapses were identified and treated as single region of interest (ROI) with a custom-made ImageJ algorithm (National Institutes of Health). Briefly, synapses were identified on the basis of their increase in signal during NH_4 application; if upon NH_4 an ROI had a $\Delta F/F_0 < 4 * \mathrm{StD}(F_0) + F_0$ where StD represents the SD of the signal, the ROI was discarded. Individual traces were analyzed with a custom-made MATLAB (MathWorks) script where synapses were quantified as active if the maximum $\Delta F/F_0$ value upon stimulation was $\geq 3 * \mathrm{StD}(F_0)$; active synapses were pooled per cell. SypHy fusion fraction was calculated as the $\Delta F_{\mathrm{stimulation}}/\Delta F_{\mathrm{NH4}}$.

For DCV fusion, 3 × 3 pixel ROIs were placed semiautomatically, using a custom-made script in ImageJ (*39*, *85*), on all pHluorin region that appeared during the electrical stimulation. Individual traces were validated using a custom-made MATLAB script (*17*, *39*), and only regions that showed an increase in $\Delta F/F_0 > 3 * \mathrm{StD}(F_0) + F_0$ and with a rise time of <1 s were considered as positive fusion events. The total number of DCVs was calculated on the basis of the NH_4Cl response of individual recording with a custom-made ImageJ algorithm. Because of the overlap of DCVs in individual puncta, the number of vesicles was corrected by normalizing the puncta intensity by the mode of the first percentile of the intensity distribution per cell. The synapsin-mCherry image was aligned to the NPY-SEP movie and segmented, and the pixel location inside the mask was used to calculate the shorted distance from the center of each 3 × 3 pixel ROI used in the DCV fusion analysis. The center of the DCV fusion ROIs was used to calculate the minimum distance between two NPY-SEP fusion events, and in the case of multiple fusion events in one ROI, the distance was set to 0.

For neuronal morphology and synaptic quantification, maximum intensity projections of confocal images were analyzed with a custom-made ImageJ algorithm, dendrites and axons based on Ridge detection and their length were calculated on the basis of the skeleton analysis in ImageJ, and synapses were identified on the basis of their intensity and dimension. For signal intensity, the intensity of each individual neuron was normalized to the average intensity of the WT condition in that biological replica. For STED quantifications, synapses and DCVs were segmented using the Iterative H-Watershed plugin of ImageJ.

For Western blot analysis, following the procedures previously described in (*39*), the band at the proper molecular weight was considered as an ROI. Intensity density was used to normalize the signal using the density of actin as reference. The adjusted signal was normalized to the signal of the WT condition.

For visualization purposes, brightness and contrast of representative examples were adjusted in a linear scale using the WT as a reference. Saturation was always <1% of the pixels, and 0% of the pixels were set to undersaturation during adjustment.

Code availability

The custom code used for data analysis in ImageJ during the current study is available in GitHub at https://github.com/alemoro.

Statistics

Anderson-Darling test was used to test the normality distribution of the data and Levene's test for homogeneity of variances. When the assumptions for parametric tests were met, *t* test and one-way analysis of variance (ANOVA) (post hoc Dunn-Sidak or Fisher) were used to test significant differences in the mean of the population. In case data were nonparametric, Mann-Whitney *U* and Kruskal-Wallis tests were used to test the significance of the median of the populations. All statistics were done in MATLAB, and their values are reported in table S1.

SUPPLEMENTARY MATERIALS

Supplementary material for this article is available at http://advances.sciencemag.org/cgi/content/full/7/21/eabf0659/DC1

View/request a protocol for this paper from *Bio-protocol*.

REFERENCES AND NOTES

1. B. L. Sabatini, W. G. Regehr, Timing of neurotransmission at fast synapses in the mammalian brain. *Nature* **384**, 170–172 (1996).
2. T. C. Sudhof, Neurotransmitter release: The last millisecond in the life of a synaptic vesicle. *Neuron* **80**, 675–690 (2013).
3. M. Y. Wong, C. Zhou, D. Shakiryanova, T. E. Lloyd, D. L. Deitcher, E. S. Levitan, Neuropeptide delivery to synapses by long-range vesicle circulation and sporadic capture. *Cell* **148**, 1029–1038 (2012).
4. T. Kim, M. C. Gondre-Lewis, I. Arnaoutova, Y. P. Loh, Dense-core secretory granule biogenesis. *Physiology* **21**, 124–133 (2006).
5. V. Bharat, M. Siebrecht, K. Burk, S. Ahmed, C. Reissner, M. Kohansal-Nodehi, V. Steubler, M. Zweckstetter, J. T. Ting, C. Dean, Capture of dense core vesicles at synapses by JNK-dependent phosphorylation of synaptotagmin-4. *Cell Rep.* **21**, 2118–2133 (2017).
6. R. van de Bospoort, M. Farina, S. K. Schmitz, A. de Jong, H. de Wit, M. Verhage, R. F. Toonen, Munc13 controls the location and efficiency of dense-core vesicle release in neurons. *J. Cell Biol.* **199**, 883–891 (2012).
7. M. Farina, R. van de Bospoort, E. He, C. M. Persoon, J. R. van Weering, J. H. Broeke, M. Verhage, R. F. Toonen, CAPS-1 promotes fusion competence of stationary dense-core vesicles in presynaptic terminals of mammalian neurons. *eLife* **4**, e12968 (2015).
8. C. M. Persoon, A. Moro, J. P. Nassal, M. Farina, J. H. Broeke, S. Arora, N. Dominguez, J. R. T. Weering, R. F. Toonen, M. Verhage, Pool size estimations for dense-core vesicles in mammalian CNS neurons. *EMBO J.* **37**, e99672 (2018).
9. R. Kolarow, T. Brigadski, V. Lessmann, Postsynaptic secretion of BDNF and NT-3 from hippocampal neurons depends on calcium calmodulin kinase II signaling and proceeds via delayed fusion pore opening. *J. Neurosci.* **27**, 10350–10364 (2007).
10. N. Matsuda, H. Lu, Y. Fukata, J. Noritake, H. Gao, S. Mukherjee, T. Nemoto, M. Fukata, M. M. Poo, Differential activity-dependent secretion of brain-derived neurotrophic factor from axon and dendrite. *J. Neurosci.* **29**, 14185–14198 (2009).
11. A. Vezzani, G. Sperk, W. F. Colmers, Neuropeptide Y: Emerging evidence for a functional role in seizure modulation. *Trends Neurosci.* **22**, 25–30 (1999).
12. L. F. Agnati, M. Zoli, I. Stromberg, K. Fuxe, Intercellular communication in the brain: Wiring versus volume transmission. *Neuroscience* **69**, 711–726 (1995).
13. J. Liu, J. K. Noel, H. H. Low, Structural basis for membrane tethering by a bacterial dynamin-like pair. *Nat. Commun.* **9**, 3345 (2018).
14. B. G. Robinson, X. Cai, J. Wang, J. R. Bunzow, J. T. Williams, P. S. Kaeser, RIM is essential for stimulated but not spontaneous somatodendritic dopamine release in the midbrain. *eLife* **8**, e47972 (2019).
15. S. Arora, I. Saarloos, R. Kooistra, R. van de Bospoort, M. Verhage, R. F. Toonen, SNAP-25 gene family members differentially support secretory vesicle fusion. *J. Cell Sci.* **130**, 1877–1889 (2017).
16. M. Shimojo, J. Courchet, S. Pieraut, N. Torabi-Rander, R. Sando III, F. Polleux, A. Maximov, SNAREs controlling vesicular release of BDNF and development of callosal axons. *Cell Rep.* **11**, 1054–1066 (2015).
17. C. M. Persoon, R. I. Hoogstraaten, J. P. Nassal, J. R. T. van Weering, P. S. Kaeser, R. F. Toonen, M. Verhage, The RAB3-RIM pathway is essential for the release of neuromodulators. *Neuron* **104**, 1065–1080.e12 (2019).
18. R. I. Hoogstraaten, L. van Keimpema, R. F. Toonen, M. Verhage, Tetanus insensitive VAMP2 differentially restores synaptic and dense core vesicle fusion in tetanus neurotoxin treated neurons. *Sci. Rep.* **10**, 10913 (2020).
19. C. Ungermann, G. F. von Mollard, O. N. Jensen, N. Margolis, T. H. Stevens, W. Wickner, Three v-SNAREs and two t-SNAREs, present in a pentameric cis-SNARE complex on isolated vacuoles, are essential for homotypic fusion. *J. Cell Biol.* **145**, 1435–1442 (1999).
20. K. Alpadi, A. Kulkarni, S. Namjoshi, S. Srinivasan, K. H. Sippel, K. Ayscough, M. Zieger, A. Schmidt, A. Mayer, M. Evangelista, F. A. Quiocho, C. Peters, Dynamin-SNARE interactions control trans-SNARE formation in intracellular membrane fusion. *Nat. Commun.* **4**, 1704 (2013).
21. A. Kulkarni, K. Alpadi, T. Sirupangi, C. Peters, A dynamin homolog promotes the transition from hemifusion to content mixing in intracellular membrane fusion. *Traffic* **15**, 558–571 (2014).
22. C. Peters, T. L. Baars, S. Buhler, A. Mayer, Mutual control of membrane fission and fusion proteins. *Cell* **119**, 667–678 (2004).
23. H. Cao, F. Garcia, M. A. McNiven, Differential distribution of dynamin isoforms in mammalian cells. *Mol. Biol. Cell* **9**, 2595–2609 (1998).
24. A. M. van der Bliek, E. M. Meyerowitz, Dynamin-like protein encoded by the *Drosophila shibire* gene associated with vesicular traffic. *Nature* **351**, 411–414 (1991).
25. K. Takei, P. S. McPherson, S. L. Schmid, P. De Camilli, Tubular membrane invaginations coated by dynamin rings are induced by GTP-γS in nerve terminals. *Nature* **374**, 186–190 (1995).
26. S. M. Ferguson, G. Brasnjo, M. Hayashi, M. Wolfel, C. Collesi, S. Giovedi, A. Raimondi, L. W. Gong, P. Ariel, S. Paradise, E. O'Toole, R. Flavell, O. Cremona, G. Miesenbock, T. A. Ryan, P. de Camilli, A selective activity-dependent requirement for dynamin 1 in synaptic vesicle endocytosis. *Science* **316**, 570–574 (2007).
27. A. Raimondi, S. M. Ferguson, X. Lou, M. Armbruster, S. Paradise, S. Giovedi, M. Messa, N. Kono, J. Takasaki, V. Cappello, E. O'Toole, T. A. Ryan, P. de Camilli, Overlapping role of dynamin isoforms in synaptic vesicle endocytosis. *Neuron* **70**, 1100–1114 (2011).
28. A. J. Newton, T. Kirchhausen, V. N. Murthy, Inhibition of dynamin completely blocks compensatory synaptic vesicle endocytosis. *Proc. Natl. Acad. Sci. U.S.A.* **103**, 17955–17960 (2006).
29. S. M. Ferguson, A. Raimondi, S. Paradise, H. Shen, K. Mesaki, A. Ferguson, O. Destaing, G. Ko, J. Takasaki, O. Cremona, E. O'Toole, P. De Camilli, Coordinated actions of actin and BAR proteins upstream of dynamin at endocytic clathrin-coated pits. *Dev. Cell* **17**, 811–822 (2009).
30. W. Shin, L. Ge, G. Arpino, S. A. Villarreal, E. Hamid, H. Liu, W.-D. Zhao, P. J. Wen, H.-C. Chiang, L.-G. Wu, Visualization of membrane pore in live cells reveals a dynamic-pore theory governing fusion and endocytosis. *Cell* **173**, 934–945.e12 (2018).
31. L. Min, Y. M. Leung, A. Tomas, R. T. Watson, H. Y. Gaisano, P. A. Halban, J. E. Pessin, J. C. Hou, Dynamin is functionally coupled to insulin granule exocytosis. *J. Biol. Chem.* **282**, 33530–33536 (2007).
32. F. Fan, C. Ji, Y. Wu, S. M. Ferguson, N. Tamarina, L. H. Philipson, X. Lou, Dynamin 2 regulates biphasic insulin secretion and plasma glucose homeostasis. *J. Clin. Invest.* **125**, 4026–4041 (2015).
33. A. Sundborger, C. Soderblom, O. Vorontsova, E. Evergren, J. E. Hinshaw, O. Shupliakov, An endophilin-dynamin complex promotes budding of clathrin-coated vesicles during synaptic vesicle recycling. *J. Cell Sci.* **124**, 133–143 (2011).
34. M. Meinecke, E. Boucrot, G. Camdere, W. C. Hon, R. Mittal, H. T. McMahon, Cooperative recruitment of dynamin and BIN/amphiphysin/Rvs (BAR) domain-containing proteins leads to GTP-dependent membrane scission. *J. Biol. Chem.* **288**, 6651–6661 (2013).
35. J. A. Ross, Y. Chen, J. Müller, B. Barylko, L. Wang, H. B. Banks, J. P. Albanesi, D. M. Jameson, Dimeric endophilin A2 stimulates assembly and GTPase activity of dynamin 2. *Biophys. J.* **100**, 729–737 (2011).
36. S. Gowrisankaran, S. Houy, J. G. P. del Castillo, V. Steubler, M. Gelker, J. Kroll, P. S. Pinheiro, D. Schwitters, N. Halbsgut, A. Pechstein, J. R. T. van Weering, T. Maritzen, V. Haucke, N. Raimundo, J. B. Sørensen, I. Milosevic, Endophilin-A coordinates priming and fusion of neurosecretory vesicles via intersectin. *Nat. Commun.* **11**, 1266 (2020).
37. R. J. Park, H. Shen, L. Liu, X. Liu, S. M. Ferguson, P. de Camilli, Dynamin triple knockout cells reveal off target effects of commonly used dynamin inhibitors. *J. Cell Sci.* **126**, 5305–5312 (2013).
38. B. Granseth, B. Odermatt, S. J. Royle, L. Lagnado, Clathrin-mediated endocytosis is the dominant mechanism of vesicle retrieval at hippocampal synapses. *Neuron* **51**, 773–786 (2006).

39. A. Moro, G. M. van Woerden, R. F. Toonen, M. Verhage, CaMKII controls neuromodulation via neuropeptide gene expression and axonal targeting of neuropeptide vesicles. *PLOS Biol.* **18**, e3000826 (2020).
40. A. Anantharam, M. A. Bittner, R. L. Aikman, E. L. Stuenkel, S. L. Schmid, D. Axelrod, R. W. Holz, A new role for the dynamin GTPase in the regulation of fusion pore expansion. *Mol. Biol. Cell* **22**, 1907–1918 (2011).
41. A. M. González-Jamett, F. Momboisse, M. J. Guerra, S. Ory, X. Báez-Matus, N. Barraza, V. Calco, S. Houy, E. Couve, A. Neely, A. D. Martínez, S. Gasman, A. M. Cárdenas, Dynamin-2 regulates fusion pore expansion and quantal release through a mechanism that involves actin dynamics in neuroendocrine chromaffin cells. *PLOS ONE* **8**, e70638 (2013).
42. E. Macia, M. Ehrlich, R. Massol, E. Boucrot, C. Brunner, T. Kirchhausen, Dynasore, a cell-permeable inhibitor of dynamin. *Dev. Cell* **10**, 839–850 (2006).
43. A. McCluskey, J. A. Daniel, G. Hadzic, N. Chau, E. L. Clayton, A. Mariana, A. Whiting, N. N. Gorgani, J. Lloyd, A. Quan, L. Moshkanbaryans, S. Krishnan, S. Perera, M. Chircop, L. von Kleist, A. B. McGeachie, M. T. Howes, R. G. Parton, M. Campbell, J. A. Sakoff, X. Wang, J. Y. Sun, M. J. Robertson, F. M. Deane, T. H. Nguyen, F. A. Meunier, M. A. Cousin, P. J. Robinson, Building a better dynasore: The dyngo compounds potently inhibit dynamin and endocytosis. *Traffic* **14**, 1272–1289 (2013).
44. J. Jackson, A. Papadopulos, F. A. Meunier, A. McCluskey, P. J. Robinson, D. J. Keating, Small molecules demonstrate the role of dynamin as a bi-directional regulator of the exocytosis fusion pore and vesicle release. *Mol. Psychiatry* **20**, 810–819 (2015).
45. C. Chung, B. Barylko, J. Leitz, X. Liu, E. T. Kavalali, Acute dynamin inhibition dissects synaptic vesicle recycling pathways that drive spontaneous and evoked neurotransmission. *J. Neurosci.* **30**, 1363–1376 (2010).
46. J. E. Hinshaw, S. L. Schmid, Dynamin self-assembles into rings suggesting a mechanism for coated vesicle budding. *Nature* **374**, 190–192 (1995).
47. H. Damke, T. Baba, D. E. Warnock, S. L. Schmid, Induction of mutant dynamin specifically blocks endocytic coated vesicle formation. *J. Cell Biol.* **127**, 915–934 (1994).
48. A. M. van der Bliek, T. E. Redelmeier, H. Damke, E. J. Tisdale, E. M. Meyerowitz, S. L. Schmid, Mutations in human dynamin block an intermediate stage in coated vesicle formation. *J. Cell Biol.* **122**, 553–563 (1993).
49. M. C. Galas, S. Chasserot-Golaz, S. Dirrig-Grosch, M. F. Bader, Presence of dynamin--syntaxin complexes associated with secretory granules in adrenal chromaffin cells. *J. Neurochem.* **75**, 1511–1519 (2000).
50. C. Zhang, A. G. Omran, F. He, X. Deng, L. Wu, J. Peng, F. Yin, Screening and identification of dynamin-1 interacting proteins in rat brain synaptosomes. *Brain Res.* **1543**, 17–27 (2014).
51. T. L. Toft-Bertelsen, I. Ziomkiewicz, S. Houy, P. S. Pinheiro, J. B. Sorensen, Regulation of Ca^{2+} channels by SNAP-25 via recruitment of syntaxin-1 from plasma membrane clusters. *Mol. Biol. Cell* **27**, 3329–3341 (2016).
52. S. Hugo, E. Dembla, M. Halimani, U. Matti, J. Rettig, U. Becherer, Deciphering dead-end docking of large dense core vesicles in bovine chromaffin cells. *J. Neurosci.* **33**, 17123–17137 (2013).
53. A. Honigmann, G. van den Bogaart, E. Iraheta, H. J. Risselada, D. Milovanovic, V. Mueller, S. Müllar, U. Diederichsen, D. Fasshauer, H. Grubmüller, S. W. Hell, C. Eggeling, K. Kühnel, R. Jahn, Phosphatidylinositol 4,5-bisphosphate clusters act as molecular beacons for vesicle recruitment. *Nat. Struct. Mol. Biol.* **20**, 679–686 (2013).
54. D. Milovanovic, M. Platen, M. Junius, U. Diederichsen, I. A. T. Schaap, A. Honigmann, R. Jahn, G. van den Bogaart, Calcium promotes the formation of syntaxin 1 mesoscale domains through phosphatidylinositol 4,5-bisphosphate. *J. Biol. Chem.* **291**, 7868–7876 (2016).
55. M. L. Wagner, L. K. Tamm, Reconstituted syntaxin1A/SNAP25 interacts with negatively charged lipids as measured by lateral diffusion in planar supported bilayers. *Biophys. J.* **81**, 266–275 (2001).
56. R. F. Toonen, K. J. de Vries, R. Zalm, T. C. Südhof, M. Verhage, Munc18-1 stabilizes syntaxin 1, but is not essential for syntaxin 1 targeting and SNARE complex formation. *J. Neurochem.* **93**, 1393–1400 (2005).
57. H. Otto, P. I. Hanson, R. Jahn, Assembly and disassembly of a ternary complex of synaptobrevin, syntaxin, and SNAP-25 in the membrane of synaptic vesicles. *Proc. Natl. Acad. Sci. U.S.A.* **94**, 6197–6201 (1997).
58. A. Mayer, W. Wickner, A. Haas, Sec18p (NSF)-driven release of Sec17p (alpha-SNAP) can precede docking and fusion of yeast vacuoles. *Cell* **85**, 83–94 (1996).
59. A. Banerjee, V. A. Barry, B. R. DasGupta, T. F. Martin, N-Ethylmaleimide-sensitive factor acts at a prefusion ATP-dependent step in Ca^{2+}–activated exocytosis. *J. Biol. Chem.* **271**, 20223–20226 (1996).
60. E. A. Prinslow, K. P. Stepien, Y. Z. Pan, J. Xu, J. Rizo, Multiple factors maintain assembled trans-SNARE complexes in the presence of NSF and αSNAP. *eLife* **8**, e38880 (2019).
61. E. He, K. Wierda, R. van Westen, J. H. Broeke, R. F. Toonen, L. N. Cornelisse, M. Verhage, Munc13-1 and Munc18-1 together prevent NSF-dependent de-priming of synaptic vesicles. *Nat. Commun.* **8**, 15915 (2017).
62. K. P. Stepien, E. A. Prinslow, J. Rizo, Munc18-1 is crucial to overcome the inhibition of synaptic vesicle fusion by αSNAP. *Nat. Commun.* **10**, 4326 (2019).
63. A. Lee, D. W. Frank, M. S. Marks, M. A. Lemmon, Dominant-negative inhibition of receptor-mediated endocytosis by a dynamin-1 mutant with a defective pleckstrin homology domain. *Curr. Biol.* **9**, 261–265 (1999).
64. J. Zheng, S. M. Cahill, M. A. Lemmon, D. Fushman, J. Schlessinger, D. Cowburn, Identification of the binding site for acidic phospholipids on the pH domain of dynamin: Implications for stimulation of GTPase activity. *J. Mol. Biol.* **255**, 14–21 (1996).
65. R. Ramachandran, T. J. Pucadyil, Y. W. Liu, S. Acharya, M. Leonard, V. Lukiyanchuk, S. L. Schmid, Membrane insertion of the pleckstrin homology domain variable loop 1 is critical for dynamin-catalyzed vesicle scission. *Mol. Biol. Cell* **20**, 4630–4639 (2009).
66. J. A. Kenniston, M. A. Lemmon, Dynamin GTPase regulation is altered by PH domain mutations found in centronuclear myopathy patients. *EMBO J.* **29**, 3054–3067 (2010).
67. Y. H. Chin, A. Lee, H. W. Kan, J. Laiman, M. C. Chuang, S. T. Hsieh, Y. W. Liu, Dynamin-2 mutations associated with centronuclear myopathy are hypermorphic and lead to T-tubule fragmentation. *Hum. Mol. Genet.* **24**, 5542–5554 (2015).
68. A. Hohendahl, A. Roux, V. Galli, Structural insights into the centronuclear myopathy-associated functions of BIN1 and dynamin 2. *J. Struct. Biol.* **196**, 37–47 (2016).
69. S. M. Ferguson, P. De Camilli, Dynamin, a membrane-remodelling GTPase. *Nat. Rev. Mol. Cell Biol.* **13**, 75–88 (2012).
70. Y. Wu, E. T. O'Toole, M. Girard, B. Ritter, M. Messa, X. Liu, P. S. McPherson, S. M. Ferguson, P. de Camilli, A dynamin 1-, dynamin 3- and clathrin-independent pathway of synaptic vesicle recycling mediated by bulk endocytosis. *eLife* **3**, e01621 (2014).
71. P. Holroyd, T. Lang, D. Wenzel, P. De Camilli, R. Jahn, Imaging direct, dynamin-dependent recapture of fusing secretory granules on plasma membrane lawns from PC12 cells. *Proc. Natl. Acad. Sci. U.S.A.* **99**, 16806–16811 (2002).
72. J. M. Lundberg, A. Rudehill, A. Sollevi, E. Theodorsson-Norheim, B. Hamberger, Frequency- and reserpine-dependent chemical coding of sympathetic transmission: Differential release of noradrenaline and neuropeptide Y from pig spleen. *Neurosci. Lett.* **63**, 96–100 (1986).
73. J. M. Lundberg, A. Rudehill, A. Sollevi, G. Fried, G. Wallin, Co-release of neuropeptide Y and noradrenaline from pig spleen in vivo: Importance of subcellular storage, nerve impulse frequency and pattern, feedback regulation and resupply by axonal transport. *Neuroscience* **28**, 475–486 (1989).
74. A. Balkowiec, D. M. Katz, Cellular mechanisms regulating activity-dependent release of native brain-derived neurotrophic factor from hippocampal neurons. *J. Neurosci.* **22**, 10399–10407 (2002).
75. T. M. Khuong, R. L. P. Habets, S. Kuenen, A. Witkowska, J. Kasprowicz, J. Swerts, R. Jahn, G. van den Bogaart, P. Verstreken, Synaptic PI(3,4,5)P3 is required for Syntaxin1A clustering and neurotransmitter release. *Neuron* **77**, 1097–1108 (2013).
76. M. Barszczewski, J. J. Chua, A. Stein, U. Winter, R. Heintzmann, F. E. Zilly, D. Fasshauer, T. Lang, R. Jahn, A novel site of action for α-SNAP in the SNARE conformational cycle controlling membrane fusion. *Mol. Biol. Cell* **19**, 776–784 (2008).
77. G. Vardar, S. Chang, M. Arancillo, Y. J. Wu, T. Trimbuch, C. Rosenmund, Distinct functions of syntaxin-1 in neuronal maintenance, synaptic vesicle docking, and fusion in mouse neurons. *J. Neurosci.* **36**, 7911–7924 (2016).
78. J. Rizo, J. Xu, The synaptic vesicle release machinery. *Annu. Rev. Biophys.* **44**, 339–367 (2015).
79. J. Rizo, Mechanism of neurotransmitter release coming into focus. *Protein Sci.* **27**, 1364–1391 (2018).
80. H. Xu, Y. Jun, J. Thompson, J. Yates, W. Wickner, HOPS prevents the disassembly of trans-SNARE complexes by Sec17p/Sec18p during membrane fusion. *EMBO J.* **29**, 1948–1960 (2010).
81. J. Emperador-Melero, V. Huson, J. van Weering, C. Bollmann, G. Fischer von Mollard, R. F. Toonen, M. Verhage, Vti1a/b regulate synaptic vesicle and dense core vesicle secretion via protein sorting at the Golgi. *Nat. Commun.* **9**, 3421 (2018).
82. S. Mennerick, J. Que, A. Benz, C. F. Zorumski, Passive and synaptic properties of hippocampal neurons grown in microcultures and in mass cultures. *J. Neurophysiol.* **73**, 320–332 (1995).
83. L. Naldini, U. Blomer, P. Gallay, D. Ory, R. Mulligan, F. H. Gage, I. M. Verma, D. Trono, In vivo gene delivery and stable transduction of nondividing cells by a lentiviral vector. *Science* **272**, 263–267 (1996).
84. P. S. Kaeser, L. Deng, A. E. Chávez, X. Liu, P. E. Castillo, T. C. Südhof, ELKS2alpha/CAST deletion selectively increases neurotransmitter release at inhibitory synapses. *Neuron* **64**, 227–239 (2009).
85. A. Moro, R. I. Hoogstraaten, C. M. Persoon, M. Verhage, R. F. Toonen, Quantitative analysis of dense-core vesicle fusion in rodent CNS neurons. *STAR Protoc.* **2**, 100325 (2021).

Acknowledgments: We thank J. Wortel for animal breeding; J. Hoetjes for genotyping; R. Zalm for cloning and producing viral particles; D. Schut for astrocyte culture and cell culture assistance; F. den Oudsten and L. Laan for astrocyte culture; I. Saarloos, A. Subkhangulova, and G. Balagura for assistance in protein chemistry and Western blot; and members of the CNCR

DCV project team, and P. De Camilli (Yale, New Haven, CT, USA) for fruitful discussions. **Funding:** This work is supported by the ERC Advanced Grant (322966) of the European Union to M.V. and NWO Gravitation program grant BRAINSCAPES (NWO 024.004.012) to M.V. **Author contributions:** Conceptualization: A.M., R.F.T., and M.V. Methodology: A.M., R.F.T., and M.V. Software: A.M. Investigation: A.M. and A.v.N. Supervision: M.V. Writing—original draft: A.M., R.F.T., and M.V. Writing—review and editing: A.M., R.F.T., and M.V. **Competing interests:** The authors declare that they have no competing interests. **Data and materials availability:** The custom code used for data analysis in ImageJ is available at https://github.com/alemoro. All data needed to evaluate the conclusions in the paper are present in the paper and/or the Supplementary Materials. The raw data used to generate the relevant figures are accessible at https://doi.org/10.34894/GZSBVP. Additional data related to this paper may be requested from the authors.

Submitted 1 October 2020
Accepted 2 April 2021
Published 21 May 2021
10.1126/sciadv.abf0659

Citation: A. Moro, A. van Nifterick, R. F. Toonen, M. Verhage, Dynamin controls neuropeptide secretion by organizing dense-core vesicle fusion sites. *Sci. Adv.* **7**, eabf0659 (2021).